13184 *J. Phys. Chem. A* **2009,** *113,* 13184–13198

Dissection of Rovibronic Structure by Polarization-Resolved Two-Color Resonant Four-Wave Mixing Spectroscopy[†]

Daniel Murdock, Lori A. Burns, and Patrick H. Vaccaro*

Department of Chemistry, Yale University, P.O. Box 208107, New Haven, Connecticut 06520-8107

Received: April 29, 2009; Revised Manuscript Received: June 17, 2009

A synergistic theoretical and experimental investigation of stimulated emission pumping (SEP) as implemented in the coherent framework of two-color resonant four-wave mixing (TC-RFWM) spectroscopy is presented, with special emphasis directed toward the identification of polarization geometries that can distinguish spectral features according to their attendant changes in rotational quantum numbers. A vector-recoupling formalism built upon a perturbative treatment of matter-field interactions and a state-multipole expansion of the density operator allowed the weak-field signal intensity to be cast in terms of a TC-RFWM response tensor, $R_Q^{(K)}(\boldsymbol{\varepsilon}_4^*\boldsymbol{\varepsilon}_3\boldsymbol{\varepsilon}_2^*\boldsymbol{\varepsilon}_1;J_g,J_e,J_h,J_f)$, which separates the transverse characteristics of the incident and generated electromagnetic waves $(\boldsymbol{\varepsilon}_4^*\boldsymbol{\varepsilon}_3\boldsymbol{\varepsilon}_2^*\boldsymbol{\varepsilon}_1)$ from the angular momentum properties of the `PUMP` and `DUMP` resonances (J_g,J_e,J_h,J_f). For an isolated SEP process induced in an isotropic medium, the criteria needed to discriminate against subsets of rovibronic structure were encoded in the roots of a single tensor element, $R_0^{(0)}(\boldsymbol{\varepsilon}_4^*\boldsymbol{\varepsilon}_3\boldsymbol{\varepsilon}_2^*\boldsymbol{\varepsilon}_1;J_g,J_e,J_h,J_e)$. By assuming all optical fields to be polarized linearly and invoking the limit of high quantum numbers, specific angles of polarization for the detected signal field were found to suppress `DUMP` resonances selectively according to the nature of their rotational branch and the rotational branch of the meshing `PUMP` line. These predictions were corroborated by performing SEP measurements on the ground electronic potential energy surface of tropolone in two distinct regimes of vibrational excitation, with the near-ultraviolet $\tilde{A}^1B_2-\tilde{X}^1A_1$ $(\pi^* \leftarrow \pi)$ absorption system affording the requisite `PUMP` and `DUMP` transitions.

I. Introduction

The frequency-domain techniques of resonant four-wave mixing (RFWM) constitute a highly versatile family of nonlinear spectroscopic tools which offer capabilities that complement and often supersede those available from their linear counterparts.[1−4] The absorption-based character of such probes eliminates the need to rely upon secondary effects (e.g., fluorescence or ionization) to locate molecular transitions, thereby making them applicable to species that possess nonradiative or short-lived excited states.[4−6] Although limited in sensitivity by the quadratic scaling of signal intensity with target number density that is the hallmark of a coherent process,[3,4] the fully resonant-enhanced nature of the underlying matter-field interactions, coupled with an essentially background-free response, has enabled RFWM to be exploited successfully in a variety of rarefied environments,[7−9] including bulk low-pressure gases and supersonic free-jet expansions. This paper focuses on the venerable method of stimulated emission pumping (SEP) as implemented in the coherent framework of two-color resonant four-wave mixing (TC-RFWM) spectroscopy. In particular, building upon prior analyses of branch-suppression schemes in degenerate four-wave mixing (DFWM),[10,11] novel polarization geometries will be introduced for the discrimination of rovibronic features according to their attendant changes in rotational quantum numbers. The feasibility and utility of this approach will be demonstrated by performing SEP measurements on the ground electronic potential energy surface of tropolone,[12,13] with the distinct behavior found in two regimes of vibrational excitation highlighting our ability to dissect and interpret congested spectral patterns.

Since its inception at the MIT laboratories of Field and Kinsey nearly three decades ago,[14] SEP has evolved into a mainstream methodology of modern-day spectroscopy.[15] This folded variant of optical-optical double resonance exploits two narrow-band sources of tunable laser light, commonly referred to as the `PUMP` and the `DUMP`, to sequentially transfer molecules from an initial thermally populated level, through an electronically excited intermediate manifold, to targeted rotation-vibration features of the ground state. The utility of this approach for studies of structure and dynamics stems from the unparalleled access that it affords to chemically relevant (i.e., vibrationally highly excited) regions of the molecular potential energy surface, with the selection rules imposed upon complementary infrared absorption techniques being supplanted by the less restrictive and, often times, more favorable considerations of Franck-Condon factors. The most common means of SEP detection rely on the competition that ensues between spontaneous and (`DUMP`-induced) stimulated emission processes acting on (`PUMP`-prepared) molecules in the intermediate state;[16] however, several alternatives to this historical fluorescence-dip (FD-SEP) scheme have been proposed, including variants based on transient gain,[17] linear birefringence/dichroism,[18] photoacoustic,[19] ionization-dip,[20] and DFWM[21,22] measurements.

The present study focuses on TC-RFWM techniques that were introduced initially under the moniker of two-color laser-induced grating spectroscopy (TC-LIGS) by Buntine, Chandler, and Hayden,[23] with key technical and conceptual innovations following from the efforts of Rohlfing and co-workers.[5,8,24] The coherent signal beam emerging from such nonlinear optical

---

[†] Part of the "Robert W. Field Festschrift".

* Corresponding author. E-mail: patrick.vaccaro@yale.edu. Phone/Fax: (203) 432-3975/(203) 432-6144.

10.1021/jp903970d CCC: $40.75

probes depends upon two distinct molecular transitions that share a common rovibronic level and are driven resonantly by the coupling of three incident electromagnetic waves. This need to simultaneously satisfy two meshing resonance conditions imparts significant species and spectral selectivity, which has been exploited profitably in a broad range of spectroscopic measurements. While previous theoretical analyses for the TC-RFWM implementation of SEP have made implicit assumptions regarding spatial isotropy of the target medium,[25,26] the ensuing discussion of polarization-based branch-suppression schemes will build upon our prior treatments of related DFWM phenomena[27] to allow examination of the more general (nonequilibrium) situation obtained in the presence of explicit angular momentum or rotational anisotropy.[28]

A variety of theoretical and experimental efforts have documented the marked influence that the polarizations of participating electromagnetic waves can exert upon the TC-RFWM process. Of special note are the extensive investigations of Williams and co-workers,[25,26] which identified configurations built upon orthogonal states of linearly polarized light (i.e., polarized horizontally or vertically along the *X*-axis or *Y*-axis, respectively, assuming collinear propagation along the *Z*-axis) that can serve to enhance certain rotationally resolved transitions with respect to others. These assertions were corroborated by SEP measurements performed on the ground electronic potential surface of the HCO radical through use of the $\tilde{B}^2A'-\tilde{X}^1A'$ origin band,[25] where the relative intensities of DUMP resonances could be modified according to the nature of their rotational branch and the rotational branch of the attendant PUMP line by selectively changing the polarization geometry (e.g., *YYXX* versus *YXXY*, where each set of adjacent letters denotes the collated transverse properties for the single detected and three incident optical fields). Lee et al. reported similar findings for TC-RFWM probes of CH in an oxyacetylene flame[29] and Br_2 in a free-jet expansion,[30] with the time-resolved studies of McCormack,[31] Settersten,[32] and their respective co-workers revealing comparable specificity. Analogous dependences on transverse field characteristics have been predicted by Costen and McKendrick for the related technique of two-color polarization spectroscopy.[33] All of these schemes lead to only partial elimination of undesired spectral features and operate best in the regime of low rotational angular momentum. In contrast, the present analyses are based upon the limit of large quantum numbers and are designed to enable entire families of rovibronic transitions to be suppressed in an essentially complete fashion.

II. Theoretical Background

The ensuing analyses of the TC-RFWM response build upon the notation and formalism introduced by our previous investigations of DFWM spectroscopy.[10,27] For simplicity, each participating electromagnetic wave is treated as being monochromatic in nature,[34] with a unique numerical index, $j = 1, 2, 3$, or 4, serving to distinguish among the incident ($j = 1, 2, 3$) and generated ($j = 4$) beams. The electric field vector, $\mathbf{E}_j(\mathbf{r},t)$, for a monochromatic plane wave having angular frequency ω_j and propagation wavevector $\mathbf{k}_j$ is given by:

$$\mathbf{E}_j(\mathbf{r},t) = \frac{1}{2}[\mathbf{E}_{\omega_j} e^{i(\mathbf{k}_j\cdot\mathbf{r}-\omega_j t)} + \mathbf{E}^*_{\omega_j} e^{-i(\mathbf{k}_j\cdot\mathbf{r}-\omega_j t)}] \qquad (1)$$

where the vector amplitude $\mathbf{E}_{\omega_j}$ can be partitioned into a constant scalar amplitude, $E_{\omega_j} = |\mathbf{E}_{\omega_j}|$, and a polarization unit vector, $\boldsymbol{\varepsilon}_j = \mathbf{E}_{\omega_j}/|\mathbf{E}_{\omega_j}|$, such that $\mathbf{E}_{\omega_j} = E_{\omega_j}\boldsymbol{\varepsilon}_j$. The corresponding cycle-averaged intensity of the electromagnetic wave, I_j, follows from:

$$I_j = \frac{c\varepsilon_0}{2} n(\omega_j) \left|E_{\omega_j}\right|^2 \qquad (2)$$

where c and ε_0 denote the speed of light and electrical permittivity for a vacuum while $n(\omega_j)$ represents the frequency-dependent index of refraction for the target medium.[35] By adopting a collinear approximation in which collimated beams propagate along the *Z*-axis of a local Cartesian reference frame (i.e., $\mathbf{k}_j \propto \hat{\mathbf{e}}_Z$) and assuming all electromagnetic waves to be polarized linearly, the transverse characteristics for each optical field can be described fully by angle ϕ_j:[27]

$$\boldsymbol{\varepsilon}_j = \cos\phi_j \hat{\mathbf{e}}_X + \sin\phi_j \hat{\mathbf{e}}_Y \qquad (3)$$

where $\hat{\mathbf{e}}_X$ and $\hat{\mathbf{e}}_Y$ denote unit vectors that span the transverse $X-Y$ plane. The branch-suppression schemes developed in this paper rely upon judicious selection of polarization geometry, as specified compactly by the ordered list of angles $\phi_4\phi_3\phi_2\phi_1 \equiv \boldsymbol{\varepsilon}_4^*\boldsymbol{\varepsilon}_3\boldsymbol{\varepsilon}_2^*\boldsymbol{\varepsilon}_1$, to eliminate a desired subset of rotationally resolved features from the TC-RFWM spectrum.

The weak-field calculation of nonlinear optical response typically relies on the framework of time-dependent perturbation theory,[3,36] where successive matter-field interactions lead to progressively higher-order terms in the resulting perturbative expansion. In the case of four-wave mixing spectroscopy, the third-order component of the induced electric polarization vector arising from the coupling of three incident fields, $\mathbf{P}^{(3)}(t)$, is responsible for creation of the observed signal photons.[4,22,37] Within the dipole approximation, this quantity can be expressed as a quantum-mechanical expectation value of the electric dipole moment operator $\boldsymbol{\mu}$:

$$\mathbf{P}^{(3)}(t) = N\,\mathrm{Tr}[\boldsymbol{\mu}\rho^{(3)}(t)] \qquad (4)$$

where N represents the number density of target species, Tr[...] signifies the trace operation taken over internal quantum states, and $\rho^{(3)}(t)$ denotes the third-order density operator obtained from perturbation theory. In the small-signal limit, where impinging electromagnetic waves remain unaffected by traversal of the molecular sample, the instantaneous four-wave mixing intensity will be directly proportional to the square modulus of $\mathbf{P}^{(3)}(t)$.[4] For nonstationary (gas-phase) media, the induced nonlinear polarization also must be averaged over translational degrees of freedom as specified by the normalized velocity distribution of the constituent particles, $f(\mathbf{v})$.[34] Under such circumstances, the overall TC-RFWM signal expression for monochromatic excitation will have the form:

$$I_4(\omega) \propto \left|\int_{\mathbf{v}} [\boldsymbol{\varepsilon}_4^*\cdot\mathbf{P}^{(3)}(\omega)] f(\mathbf{v})\,\mathrm{d}\mathbf{v}\right|^2 \qquad (5)$$

where $I_4(\omega)$ denotes the frequency-dependent intensity of the signal field emerging with polarization characteristics specified by unit vector $\boldsymbol{\varepsilon}_4$ and $\boldsymbol{\varepsilon}_4^*\cdot\mathbf{P}^{(3)}(\omega)$ represents the Fourier transform of the analogous time-dependent quantity, $\boldsymbol{\varepsilon}_4^*\cdot\mathbf{P}^{(3)}(t)$.

The variant of TC-RFWM spectroscopy exploited for the present frequency-domain studies is depicted in Figure 1. This scheme builds upon the venerable SEP technique by utilizing

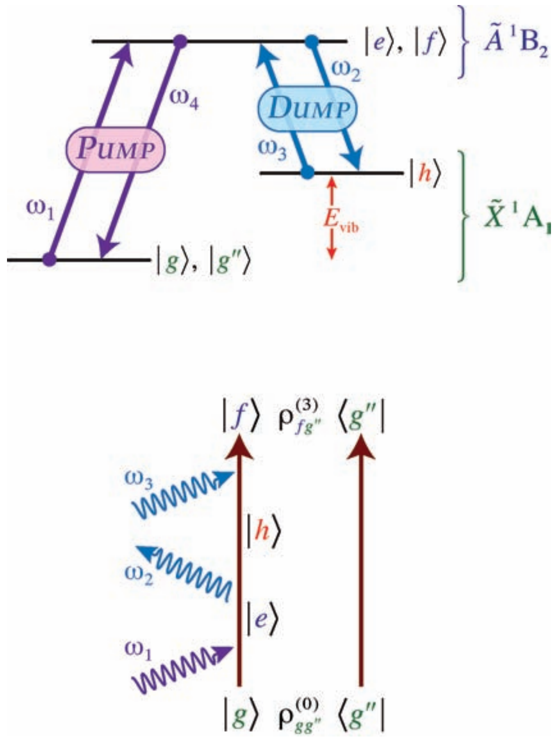

Figure 1. TC-RFWM implementation of SEP spectroscopy. The energy level pattern (top) and perturbative Feynman diagram (bottom) for our TC-RFWM implementation of SEP are presented, showing how a concerted sequence of matter-field interactions transforms three input waves (ω_1, ω_2, ω_3) into the emerging signal field (ω_4). A single `PUMP` beam (ω_1) links the initial ground-state manifold ($|g\rangle$, $|g''\rangle$) with the electronically excited intermediate state ($|e\rangle$, $|f\rangle$), before two degenerate `DUMP` beams (ω_2 and ω_3) induce transitions that probe the targeted vibrational level ($|h\rangle$ of energy E_{vib}) within the ground electronic potential surface. A pictorial representation of the single time-ordered process responsible for the resulting TC-RFWM response can be found in the double-sided Feynman diagram, where time is defined to increase from bottom to top with the correlated evolution of conjugate bra and ket spaces being symbolized by the two vertical arrows. Each coupling with an applied field, denoted by a wavy arrow directed to indicated absorption (pointing inward) or emission (pointing outward) events, gives rise to a successively higher-order term in the perturbative expansion of the molecular density operator, ultimately describing the transformation of $\rho^{(0)}_{gg''}$ into its third-order counterpart, $\rho^{(3)}_{fg''}$.

two high-resolution sources of tunable laser radiation (viz., the `PUMP` and the `DUMP`) to coherently drive a folded optical-optical double-resonance process designed to interrogate vibrationally excited portions of the ground potential energy surface. A single `PUMP` beam having frequency and wavevector specified by (ω_1,$\mathbf{k}_1$) is tuned to coincide with an isolated rovibronic feature, thereby accessing preselected eigenstates within the electronically excited manifold. Two `DUMP` beams, characterized by (ω_2,$\mathbf{k}_2$) and (ω_3,$\mathbf{k}_3$) with $\omega_2 = \omega_3$, subsequently are scanned to locate coupled transitions that terminate on the targeted vibrational levels of the ground state. Nonlinear phenomena enhanced strongly by resonant interaction with the molecular sample give rise to a signal wave that is restricted by energy conservation to be degenerate with the `PUMP` field, $\omega_4 = \omega_1 - \omega_2 + \omega_3$. While many possible arrangements of input and output beams can be envisioned, the advantages afforded by the forward-box phase-matching geometry have made it a staple in four-wave mixing experiments.[4,5,8] Here, the three incident beams ($j = 1$, 2, 3) are directed through the target medium in a nearly copropagating fashion such that they traverse distinct major diagonals of a rectangular parallelepiped (or box), with their region of mutual intersection defining the sample interaction volume. Conservation of linear momentum leads to constructive interference of the TC-RFWM signal field ($j = 4$) along a specific spatial direction, $\mathbf{k}_4 = \mathbf{k}_1 - \mathbf{k}_2 + \mathbf{k}_3$, which roughly coincides with the "dark" axis of detection defined by the remaining diagonal of the box.[5] This phase-matching configuration greatly enhances the ability to discriminate signal photons from more intense sources of scattered background light.

As depicted in Figure 1, it proves convenient to consider an isolated sequence of one-photon transitions taking place between quantum states distinguished by labels "*g*" (for the initial ground electronic state), "*e*" and "*f*" (for the intermediate electronically excited state), and "*h*" (for the vibrationally excited ground electronic state). The corresponding eigenbasis for the unperturbed molecular Hamiltonian can be specified fully by $|\alpha\rangle \equiv |\eta_\alpha J_\alpha M_\alpha\rangle$ ($\alpha = g, e, f, h$), where M_α denotes the projection of total angular momentum J_α on the space-fixed quantization axis and η_α represents all other rovibronic quantum numbers, with primes serving to differentiate the magnetic sublevels comprising each $(2J_\alpha + 1)$-fold degenerate manifold (e.g., $|g\rangle \equiv |\eta_g J_g M_g\rangle$ and $|g''\rangle \equiv |\eta_g J_g M''_g\rangle$). The rest angular frequency, $\omega_{\alpha\beta}$, and the phenomenological damping rate, $\Gamma_{\alpha\beta}$, for the $|\alpha\rangle \leftrightarrow |\beta\rangle$ resonance follow from:

$$\omega_{\alpha\beta} = \frac{1}{\hbar}(E_\alpha - E_\beta) \tag{6}$$

$$\Gamma_{\alpha\beta} = \frac{1}{2}(\Gamma_{\alpha\alpha} - \Gamma_{\beta\beta}) + \Gamma^{\phi}_{\alpha\beta} \tag{7}$$

where E_α and $\Gamma_{\alpha\alpha}$ denote the unperturbed energy and the depopulation rate, respectively, for quantum state $|\alpha\rangle$, while $\Gamma^{\phi}_{\alpha\beta}$ describes the rate of pure dephasing processes that destroy molecular coherence without disrupting corresponding populations.[3] Typically, $\eta_f = \eta_e$ and $J_f = J_e$, such that $|f\rangle$ and $|e\rangle$ represent magnetic sublevels within the same rovibronic eigenstate of the electronically excited potential surface; however, these conditions, leading to degenerate pairs of `PUMP` ($\omega_{fg} = \omega_{eg}$) and `DUMP` ($\omega_{fh} = \omega_{eh}$) transition frequencies, are not essential for a valid RFWM pathway (*vide infra*). Only quantum states composing the $|g\rangle$ manifold, $\{|\eta_g J_g M_g\rangle;\ M_g = -J_g, \ldots, J_g\}$, are assumed to be populated prior to the four-wave mixing interaction, with the distribution and correlation of probability amplitude among magnetic sublevels being specified fully by matrix elements of the unperturbed (zero-order) density operator, $\rho^{(0)}(\eta_g J_g)$:[38]

$$\begin{aligned}\rho^{(0)}_{gg''}(\eta_g J_g) &= \langle g|\rho^{(0)}(\eta_g J_g)|g''\rangle \\ &= \langle \eta_g J_g M_g|\rho^{(0)}(\eta_g J_g)|\eta_g J_g M''_g\rangle\end{aligned} \tag{8}$$

The arguments appearing in $\rho^{(0)}(\eta_g J_g)$ reflect the diagonal nature of this time-independent operator with respect to quantum numbers η_g and J_g. For an equilibrated ensemble of molecules, where the occupancy of magnetic sublevels is expected to be uniform and incoherent, the total population of the initial rovibronic level, $N \equiv N_{\eta_g J_g}$, will be distributed evenly among the $(2J_g + 1)$-fold degenerate manifold of eigenstates such that $\rho^{(0)}_{gg''}(\eta_g J_g) = \delta_{gg''}/(2J_g + 1)$, where δ_{ij} denotes the Kronecker Delta function (viz., $\delta_{ij} = 1$ if $i = j$ and zero otherwise).

The explicit form of $\rho^{(3)}(t)$ needed for evaluation of the nonlinear polarization $\mathbf{P}^{(3)}(t)$ follows from solution of the Liouville equation that governs evolution of the target medium under the influence of applied electromagnetic waves and intrinsic relaxation pathways.[3,38] Diagrammatic techniques[3,39] are especially useful for organizing and interpreting the matter-field couplings responsible for successive transformation of $\rho^{(0)}(\eta_g J_g)$ into its third-order counterpart, $\rho^{(3)}(t)$, with the lone double-sided Feynman diagram of Figure 1 affording a blueprint for the perturbative scheme relevant to the present analyses. In particular, provided that the initial population of molecules is restricted to the ground-state manifold (cf., eq 8), this specific time ordering of interactions is the *only* combination of one-photon resonant processes that generates signal photons having the temporal (ω_4) and spatial ($\mathbf{k}_4$) characteristics appropriate for our TC-RFWM implementation of SEP spectroscopy.[25,26] A straightforward, albeit tedious, calculation performed under the assumption of monochromatic excitation leads to:[4]

$$\rho^{(3)}(t) = \frac{1}{8\hbar^3} E_{\omega_1} E^*_{\omega_2} E_{\omega_3} e^{i(\mathbf{k}_\sigma \cdot \mathbf{r} - \omega_\sigma t)} \sum_{g,g''} |f\rangle \rho^{(0)}_{gg''}(\eta_g J_g) \langle g''| \times \sum_{e,h,f} \frac{\langle f|\boldsymbol{\varepsilon}_3 \cdot \boldsymbol{\mu}|h\rangle \langle h|\boldsymbol{\varepsilon}^*_2 \cdot \boldsymbol{\mu}|e\rangle \langle e|\boldsymbol{\varepsilon}_1 \cdot \boldsymbol{\mu}|g\rangle}{(\Omega_{eg''} - \omega_1)(\Omega_{hg''} - \omega_1 + \omega_2)(\Omega_{fg''} - \omega_1 + \omega_2 - \omega_3)} \tag{9}$$

where $\mathbf{k}_\sigma = \mathbf{k}_1 - \mathbf{k}_2 + \mathbf{k}_3$, $\omega_\sigma = \omega_1 - \omega_2 + \omega_3$, and the complex quantities $\Omega_{\alpha\beta} = \omega_{\alpha\beta} - i\Gamma_{\alpha\beta}$ embody both the angular frequency and the dephasing rate for the $|\alpha\rangle \leftrightarrow |\beta\rangle$ transition. By substituting this form for $\rho^{(3)}(t)$ into the expectation value of eq 4 and Fourier transforming the resulting expression for $\boldsymbol{\varepsilon}^*_4 \cdot \mathbf{P}^{(3)}(t)$ into the frequency domain, the TC-RFWM signal polarization becomes:

$$\boldsymbol{\varepsilon}^*_4 \cdot \mathbf{P}^{(3)}(\omega) = \frac{N_{\eta_g J_g}}{8\hbar^3} E_{\omega_1} E^*_{\omega_2} E_{\omega_3} e^{i\mathbf{k}_\sigma \cdot \mathbf{r}}\, \delta(\omega - \omega_\sigma) \sum_{g,g''} \rho^{(0)}_{gg''}(\eta_g J_g) \times \sum_{e,h,f} \frac{\langle g''|\boldsymbol{\varepsilon}^*_4 \cdot \boldsymbol{\mu}|f\rangle \langle f|\boldsymbol{\varepsilon}_3 \cdot \boldsymbol{\mu}|h\rangle \langle h|\boldsymbol{\varepsilon}^*_2 \cdot \boldsymbol{\mu}|e\rangle \langle e|\boldsymbol{\varepsilon}_1 \cdot \boldsymbol{\mu}|g\rangle}{(\Omega_{eg''} - \omega_1)(\Omega_{hg''} - \omega_1 + \omega_2)(\Omega_{fg''} - \omega_1 + \omega_2 - \omega_3)} \times \tag{10}$$

where the Dirac Delta function, $\delta(\omega - \omega_\sigma)$, reflects the imposition of energy conservation criteria, $\omega \longmapsto \omega_\sigma \equiv \omega_4$, while the complex exponential, $e^{i\mathbf{k}_\sigma \cdot \mathbf{r}}$, embodies the constraints of linear momentum conservation, $\mathbf{k} \longmapsto \mathbf{k}_\sigma \equiv \mathbf{k}_4$.[40]

The TC-RFWM signal polarization in eq 10 contains the product of four one-photon electric dipole moment matrix elements, $\langle \alpha|\boldsymbol{\varepsilon}_j \cdot \boldsymbol{\mu}|\beta\rangle$, scaled by a resonant denominator factor,

$$D(\omega;\omega_1,-\omega_2,\omega_3) = \frac{\delta(\omega - \omega_\sigma)}{(\Omega_{eg''} - \omega_1)(\Omega_{hg''} - \omega_1 + \omega_2)(\Omega_{fg''} - \omega_1 + \omega_2 - \omega_3)} \tag{11}$$

which encodes the intrinsic frequency response of the four-wave mixing process.[34] These quantities can be decoupled from one another by recognizing that magnetic sublevels are degenerate ($E_\alpha = E_{\alpha'}$ such that $\omega_{\alpha\beta} = \omega_{\alpha'\beta'} = -\omega_{\beta\alpha}$) and assuming that relaxation processes take place in an isotropic fashion ($\Gamma_{\alpha\alpha} = \Gamma_{\alpha'\alpha'}$ with $\Gamma_{\alpha\beta} = \Gamma_{\alpha'\beta'} = \Gamma_{\beta\alpha}$).[27] Under such circumstances, $\Omega_{\alpha\beta} = \Omega_{\alpha'\beta'} = -\Omega^*_{\beta\alpha}$ and the TC-RFWM signal polarization becomes:

$$\boldsymbol{\varepsilon}^*_4 \cdot \mathbf{P}^{(3)}(\omega) = \frac{N_{\eta_g J_g}}{8\hbar^3} E_{\omega_1} E^*_{\omega_2} E_{\omega_3} e^{i\mathbf{k}_\sigma \cdot \mathbf{r}} \langle O_{4321}\rangle D(\omega;\omega_1,-\omega_2,\omega_3) \tag{12}$$

where $\langle O_{4321}\rangle$ denotes the expectation value of a 4-fold transition dipole operator, O_{4321}:[27]

$$\begin{aligned} \langle O_{4321}\rangle &= \mathrm{Tr}[\rho^{(0)}(\eta_g J_g) O_{4321}] \\ &= \sum_{g,g''} \rho^{(0)}_{gg''}(\eta_g J_g) \times \\ &\quad \sum_{e,h,f} \langle g''|\boldsymbol{\varepsilon}^*_4 \cdot \boldsymbol{\mu}|f\rangle \langle f|\boldsymbol{\varepsilon}_3 \cdot \boldsymbol{\mu}|h\rangle \langle h|\boldsymbol{\varepsilon}^*_2 \cdot \boldsymbol{\mu}|e\rangle \langle e|\boldsymbol{\varepsilon}_1 \cdot \boldsymbol{\mu}|g\rangle \end{aligned} \tag{13}$$

The formal definition for O_{4321} can be given in terms of normalized projection operators onto the $(2J_\alpha + 1)$-dimensional subspace spanned by eigenvectors $\{|\eta_\alpha J_\alpha M_\alpha\rangle; M_\alpha = -J_\alpha,..., J_\alpha\}$,

$$P_\alpha = \sum_{M_\alpha} |\eta_\alpha J_\alpha M_\alpha\rangle \langle \eta_\alpha J_\alpha M_\alpha| \tag{14}$$

such that:[27]

$$O_{4321} = (\boldsymbol{\varepsilon}^*_4 \cdot \boldsymbol{\mu}) P_f (\boldsymbol{\varepsilon}_3 \cdot \boldsymbol{\mu}) P_h (\boldsymbol{\varepsilon}^*_2 \cdot \boldsymbol{\mu}) P_e (\boldsymbol{\varepsilon}_1 \cdot \boldsymbol{\mu}) \tag{15}$$

Further refinement of the TC-RFWM signal expression relies upon the vector-recoupling formalism,[37,41] which affords a powerful and versatile tool for systematically unraveling the spatial properties of resonant matter-field interactions. This approach exploits the inherent symmetries of irreducible spherical tensors[38,42] to bring about a near-complete separation of the induced optical response into contributions arising from dynamical (e.g., molecular moments and populations) and geometrical (e.g., input/output field polarizations) factors. A detailed discussion of the procedures required to effect such transformations in the case of DFWM has been reported by Wasserman et al.,[27] with straightforward extension of these analyses to our TC-RFWM implementation of SEP spectroscopy showing that eq 13 can be written as:

$$\langle O_{4321}\rangle = \mu^*_{fg} \mu_{fh} \mu^*_{eh} \mu_{eg} \times \sum_{K=0}^{2J_g \leq 4} \sum_{Q=-K}^{K} \langle T^{(K)}_Q(\eta_g J_g)^\dagger\rangle\, R^{(K)}_Q(\boldsymbol{\varepsilon}^*_4 \boldsymbol{\varepsilon}_3 \boldsymbol{\varepsilon}^*_2 \boldsymbol{\varepsilon}_1; J_g, J_e, J_h, J_f) \tag{16}$$

where $\mu_{\alpha\beta} \equiv \langle \eta_\alpha J_\alpha \| T^{(1)}(\boldsymbol{\mu}) \| \eta_\beta J_\beta\rangle$ is a reduced matrix element for the electric dipole operator which has been recast as a irreducible spherical tensor of rank one, $T^{(1)}(\boldsymbol{\mu})$. Expansion of the unperturbed density operator in terms of geometrical tensors has introduced the state-multipole moments,[38] $\langle T^{(K)}_Q(\eta_g J_g)^\dagger\rangle$, a set of complex coefficients that describe the initial distribution and correlation of probability amplitude among ground-state magnetic sublevels. Of special importance for the present work is the TC-RFWM response tensor, $R^{(K)}_Q(\boldsymbol{\varepsilon}^*_4 \boldsymbol{\varepsilon}_3 \boldsymbol{\varepsilon}^*_2 \boldsymbol{\varepsilon}_1; J_g, J_e, J_h, J_f)$, a fully calculable quantity that embodies the angular momentum properties of the targeted SEP process (J_g, J_e, J_h, J_f) as well as the transverse characteristics of the incident and generated electromagnetic waves ($\boldsymbol{\varepsilon}^*_4 \boldsymbol{\varepsilon}_3 \boldsymbol{\varepsilon}^*_2 \boldsymbol{\varepsilon}_1$). Detailed analyses show that $R^{(K)}_Q(\boldsymbol{\varepsilon}^*_4 \boldsymbol{\varepsilon}_3 \boldsymbol{\varepsilon}^*_2 \boldsymbol{\varepsilon}_1; J_g, J_e, J_h, J_f)$ can be formulated as a double summation taken over the products of geometrical factors, $G(J_g, J_e, J_h, J_f; \kappa_1, \kappa_2, K)$, with elements of the field polarization tensor, $F^{(K)}_Q(\boldsymbol{\varepsilon}^*_4 \boldsymbol{\varepsilon}_3 \boldsymbol{\varepsilon}^*_2 \boldsymbol{\varepsilon}_1; \kappa_1, \kappa_2)$:

$$R_Q^{(K)}(\boldsymbol{\varepsilon}_4^*\boldsymbol{\varepsilon}_3\boldsymbol{\varepsilon}_2^*\boldsymbol{\varepsilon}_1;J_g,J_e,J_h,J_f) = \sum_{\kappa_1=0}^{2}\sum_{\kappa_2=0}^{2} G(J_g,J_e,J_h,J_f;\kappa_1,\kappa_2,K)F_Q^{(K)}(\boldsymbol{\varepsilon}_4^*\boldsymbol{\varepsilon}_3\boldsymbol{\varepsilon}_2^*\boldsymbol{\varepsilon}_1;\kappa_1,\kappa_2) \tag{17}$$

Wasserman et al. have provided a formal definition for $F_Q^{(K)}(\boldsymbol{\varepsilon}_4^*\boldsymbol{\varepsilon}_3\boldsymbol{\varepsilon}_2^*\boldsymbol{\varepsilon}_1;\kappa_1,\kappa_2)$, highlighting its dependence on the polarization and phase-matching configuration adopted for a given four-wave mixing measurement.[27] Evaluation of the $G(J_g,J_e,J_h,J_f;\kappa_1,\kappa_2,K)$ factors, which reflect the angular momentum changes accompanying a TC-RFWM process ($J_g \rightarrow J_e \rightarrow J_h \rightarrow J_f \rightarrow J_g$), requires extension of the analogous DFWM expression derived by these authors:

$$G(J_g,J_e,J_h,J_f;\kappa_1,\kappa_2,K) = (-1)^{\kappa_1+\kappa_2+J_e+J_h+J_f-J_g}\sqrt{(2\kappa_1+1)(2\kappa_2+1)} \times \begin{Bmatrix} \kappa_1 & \kappa_2 & K \\ J_g & J_g & J_h \end{Bmatrix}\begin{Bmatrix} 1 & 1 & \kappa_1 \\ J_g & J_h & J_f \end{Bmatrix}\begin{Bmatrix} 1 & 1 & \kappa_2 \\ J_g & J_h & J_e \end{Bmatrix} \tag{18}$$

where the curly brackets represent Wigner 6−J symbols,[42] the symmetry properties of which show that the possible values of J_h are limited to J_g, $J_g \pm 1$, and $J_g \pm 2$ (for $0 \leq \kappa_i \leq 2$).

By redefining the induced TC-RFWM polarization $\boldsymbol{\varepsilon}_4^* \cdot \mathbf{P}^{(3)}(\omega)$ in terms of the vector-recoupled form for $\langle O_{4321}\rangle$, the monochromatic signal expression of eq 5 becomes:

$$I_4(\omega) \propto N_{\eta_g J_g}^2 \left|\mu_{fg}\right|^2\left|\mu_{fh}\right|^2\left|\mu_{eh}\right|^2\left|\mu_{eg}\right|^2 I_1 I_2 I_3\, L(\omega) \times \left|\sum_{K=0}^{4\leq 2J_g}\sum_{Q=-K}^{K}\langle T_Q^{(K)}(\eta_g J_g)^\dagger\rangle R_Q^{(K)}(\boldsymbol{\varepsilon}_4^*\boldsymbol{\varepsilon}_3\boldsymbol{\varepsilon}_2^*\boldsymbol{\varepsilon}_1;J_g,J_e,J_h,J_f)\right|^2 \tag{19}$$

which displays the expected dependence of weak-field response on the square of the target number density ($N_{\eta_g J_g}^2$) and the product of incident field intensities ($I_j \propto |E_{\omega_j}|^2$).[3,4] For the usual case of $\eta_f = \eta_e$ and $J_f = J_e$, the reduced matrix elements in $I_4(\omega)$ collapse to give $|\mu_{eh}|^4|\mu_{eg}|^4$, showing that the signal intensity will scale quadratically with the independent transition strengths ($\propto|\mu_{\alpha\beta}|^2$) for the PUMP ($|e\rangle \leftrightarrow |g\rangle$) and the DUMP ($|e\rangle \leftrightarrow |h\rangle$) resonances. The characteristic spectral response of TC-RFWM follows from the velocity-averaged lineshape function $L(\omega)$:

$$L(\omega) = \left|\int_{\mathbf{v}} D(\omega;\omega_1,-\omega_2,\omega_3)f(\mathbf{v})\,\mathrm{d}\mathbf{v}\right|^2 \tag{20}$$

where the frequency of each impinging electromagnetic wave in the resonant denominator factor of eq 11 must be replaced by its Doppler shifted analog, $\omega_j \rightarrow \omega_j - \mathbf{k}_j\cdot\mathbf{v}$.

Equation 19 provides a general solution for the monochromatic TC-RFWM signal intensity generated when the SEP process of Figure 1 takes place in a medium possessing intrinsic angular momentum anisotropy, as defined by nonvanishing multipole moments, $\langle T_Q^{(K)}(\eta_g J_g)^\dagger\rangle$, of rank $K > 0$.[38,42] Consequently, this expression should be applicable to a variety of experimental measurements performed on nonequilibrated ensembles of target molecules that display net orientation and/or alignment,[28,41] including state-resolved probes of the nascent products emerging from chemical reactions and photofragmentation events. Although not developed further in the present work, the requisite higher-order components of the TC-RFWM response tensor, which collectively govern the spectral manifestation of such rotational anisotropy effects, can be computed readily from the definitions given in eqs 17 and 18.

Substantial simplification of eq 19 can be realized in the case of a rotationally isotropic medium, where the absence of molecular coherences and the uniform population of magnetic sublevels demand that only the rank-zero ($K = 0$) monopole moment exists:[38]

$$\langle T_Q^{(K)}(\eta_g J_g)^\dagger\rangle = \delta_{K0}\delta_{Q0}(2J_g+1)^{-1/2} \tag{21}$$

Under such circumstances, the SEP signal intensity will be proportional to the square modulus of a single TC-RFWM response tensor element:

$$I_4(\omega) \propto \frac{N_{\eta_g J_g}^2}{2J_g+1}\left|\mu_{fg}\right|^2\left|\mu_{fh}\right|^2\left|\mu_{eh}\right|^2\left|\mu_{eg}\right|^2 \times \left|R_0^{(0)}(\boldsymbol{\varepsilon}_4^*\boldsymbol{\varepsilon}_3\boldsymbol{\varepsilon}_2^*\boldsymbol{\varepsilon}_1;J_g,J_e,J_h,J_f)\right|^2 I_1 I_2 I_3\, L(\omega) \tag{22}$$

The systematic disappearance of $R_0^{(0)}(\boldsymbol{\varepsilon}_4^*\boldsymbol{\varepsilon}_3\boldsymbol{\varepsilon}_2^*\boldsymbol{\varepsilon}_1;J_g,J_e,J_h,J_f)$ for certain combinations of incident/detected field polarizations and PUMP/DUMP rotational branches affords the basis for the isotropic TC-RFWM suppression schemes introduced by the present study. Assuming all electromagnetic waves to be polarized linearly such that $\boldsymbol{\varepsilon}_4^*\boldsymbol{\varepsilon}_3\boldsymbol{\varepsilon}_2^*\boldsymbol{\varepsilon}_1 \equiv \phi_4\phi_3\phi_2\phi_1$ and neglecting complications incurred by slight deviations from exactly collinear propagation,[27] the requisite elements of the rank-zero response tensor can be formulated as:

$$(2J_g+1)^{3/2}R_0^{(0)}(\phi_4\phi_3\phi_2\phi_1;J_g,J_e,J_h,J_f) = \frac{1}{60c_{00}}[c_{12}\cos(\phi_1+\phi_2-\phi_3-\phi_4) + c_{13}\cos(\phi_1-\phi_2+\phi_3-\phi_4) + c_{14}\cos(\phi_1-\phi_2-\phi_3+\phi_4)] \tag{23}$$

where each component has been scaled by a common factor of $(2J_g+1)^{3/2}$. The coefficients appearing in this expression (c_{00}, c_{12}, c_{13}, and c_{14}) are polynomials in J_g that reflect the changes in angular momentum quantum numbers (ΔJ_{eg}, ΔJ_{eh}, and ΔJ_{fh}) taking place during the four-wave mixing interaction. Table 1 contains a compilation of these quantities for $\eta_f = \eta_e$ and $J_f = J_e$ (which implies $\Delta J_{fh} = \Delta J_{eh}$). The resulting SEP processes can be labeled conveniently by the juxtaposition of two letters (e.g., *PQ*) that specify the rotational branches for the PUMP (ΔJ_{eg}) and the DUMP (ΔJ_{eh}) transitions, $\{\Delta J_{eg}\}\{\Delta J_{eh}\}$, where the symbol $\{\Delta J_{\alpha\beta}\}$ assumes the designation "*P*", "*Q*", or "*R*" depending on whether the corresponding value of $\Delta J_{\alpha\beta}$ is equal to −1, 0, or +1, respectively. As discussed in section IV, judicious selection of field polarizations will lead to a branch-specific suppression of the rank-zero response tensor element, thus providing a handle for the controlled manipulation of rovibronic intensities in TC-RFWM spectroscopy. Expansion coefficients for eq 23 that encompass the more general situation of $\Delta J_{fh} \neq \Delta J_{eh}$ can be found in Tables 3−5.

III. Experiment

Figure 2 schematically illustrates the basic experimental configuration employed for demonstration of TC-RFWM branch-

TABLE 1: Expansion Coefficients for TC-RFWM Response Tensor[a]

transition designation			coefficients for scaled rank-zero TC-RFWM response tensor				
label	ΔJ_{eg}	ΔJ_{eh}	c_{00}	c_{12}	c_{13}	c_{14}	restriction
PP	−1	−1	$J_g(2J_g - 1)$	$(J_g + 1)(2J_g + 3)$	$2(6J_g^2 - 1)$	$(J_g - 1)(2J_g - 3)$	$J_g \geq 1$
PQ	−1	0	$J_g(2J_g - 1)$	$3(J_g + 1)(2J_g + 1)$	$(2J_g + 1)(3J_g - 2)$	$-(2J_g + 1)(2J_g - 3)$	$J_g \geq 1$
PR	−1	+1	$(2J_g - 1)$	$6(2J_g + 1)$	$(2J_g + 1)$	$(2J_g + 1)$	$J_g \geq 2$
QP	0	−1	$(J_g + 1)$	$3(J_g + 2)$	$(3J_g + 1)$	$-(2J_g - 1)$	$J_g \geq 1$
QQ	0	0	$J_g(J_g + 1)$	$4J_g(J_g + 1) - 3$	$4J_g(J_g + 1) + 2$	$4J_g(J_g + 1) - 3$	$J_g \geq 1$
QR	0	+1	J_g	$3(J_g - 1)$	$(3J_g + 2)$	$-(2J_g + 3)$	$J_g \geq 1$
RP	+1	−1	$(2J_g + 3)$	$6(2J_g + 1)$	$(2J_g + 1)$	$(2J_g + 1)$	
RQ	+1	0	$(J_g + 1)(2J_g + 3)$	$3J_g(2J_g + 1)$	$(2J_g + 1)(3J_g + 5)$	$-(2J_g + 1)(2J_g + 5)$	
RR	+1	+1	$(J_g + 1)(2J_g + 3)$	$J_g(2J_g - 1)$	$12J_g(J_g + 2) + 10$	$(J_g + 2)(2J_g + 5)$	

[a] The dimensionless expansion coefficients needed to describe the rank-zero element of the scaled TC-RFWM response tensor in eq 23 are tabulated as a function of the initial rotational quantum number J_g, with results being partitioned according to the angular momentum changes induced by the PUMP (ΔJ_{eg}) and the DUMP (ΔJ_{eh}) transitions.

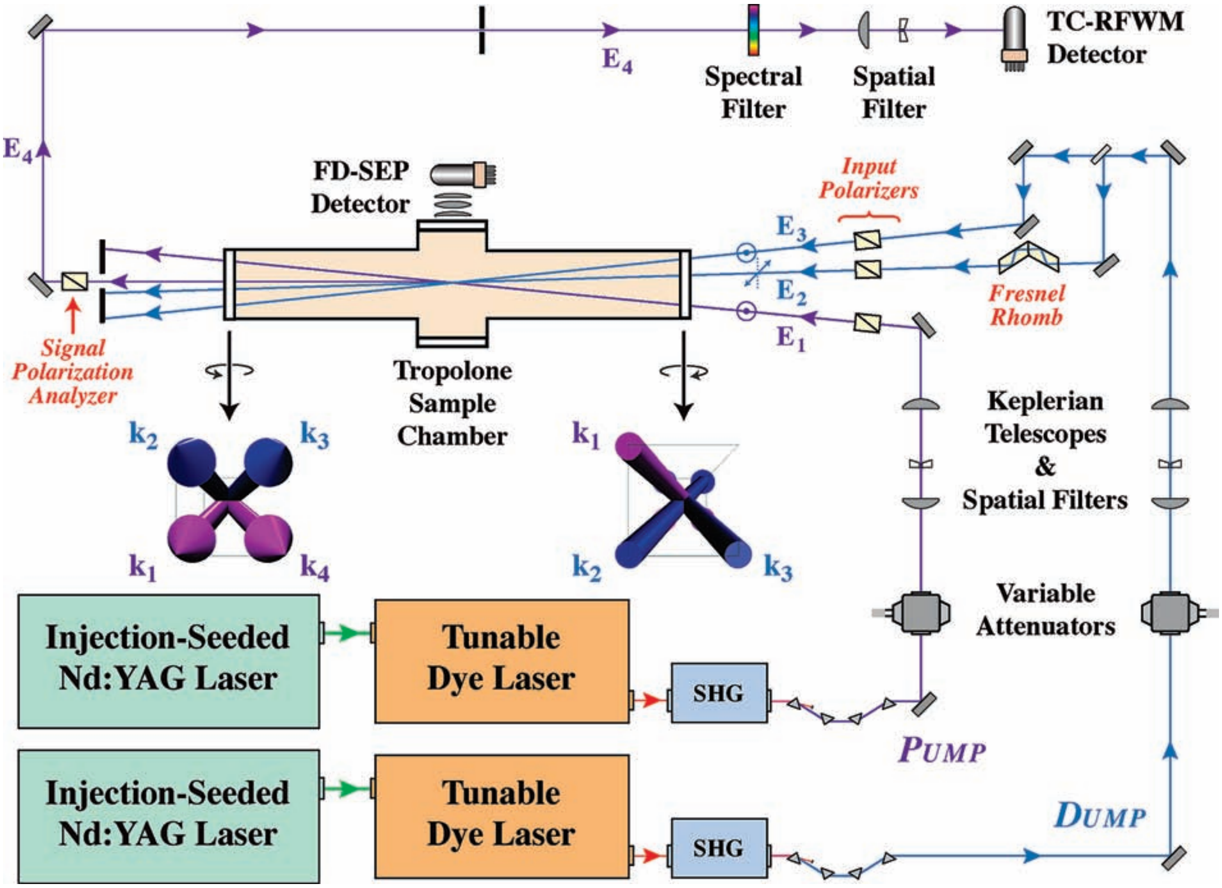

Figure 2. Experimental configuration. The experimental apparatus employed for TC-RFWM studies of ambient tropolone vapor is depicted schematically. Tunable ultraviolet radiation produced by two high-resolution dye lasers was partitioned into the three input beams, $\mathbf{E}_1(\omega_1,\mathbf{k}_1)$, $\mathbf{E}_2(\omega_2,\mathbf{k}_2)$, and $\mathbf{E}_3(\omega_3,\mathbf{k}_3)$ ($\omega_2 = \omega_3 < \omega_1$), needed to implement the forward-box phase-matching configuration, with the emerging signal photons, $\mathbf{E}_4(\omega_4,\mathbf{k}_4)$ ($\omega_4 = \omega_1$), being isolated through use of spectral and spatial filters. Optical components inserted into the paths traversed by incident and detected waves permitted various arrangements of linear polarization to be established, as required for the rovibronic branch-suppression methodology discussed in the text. Attempts to simultaneously record fluorescence-dip SEP (FD-SEP) data did not yield any discernible spectral features.

suppression geometries. Tunable electromagnetic radiation was generated by using the second harmonics of two injection-seeded Nd:YAG systems (Spectra-Physics PRO-250-20 and PRO-270-20; 20 pps repetition rate; ~10 ns pulse duration) to separately pump a pair of high-resolution dye lasers (Lambda Physik FL3002E and ScanMate 2E containing methanol solutions of Exciton LDS 751 and LDS 765 dyes, respectively). For each of these sources, the time-averaged bandwidth was reduced to ~0.035 cm^{-1} by inserting an intracavity etalon that could be scanned synchronously (under external computer control) with an intracavity diffraction grating. The independently tunable outputs from the dye lasers were frequency-doubled by means of servo-locked BBO crystals (Inrad AutoTracker II) to yield ultraviolet radiation in the vicinity of 370 nm (for the PUMP) and 390 nm (for the DUMP), with small fractions of residual fundamental light being sent to heated iodine absorption cells (for absolute frequency calibration) and monitor etalons (for scan linearization and laser diagnostics). Following isolation by Brewster-angle prisms, the PUMP and DUMP propagated through Keplerian telescopes where they were spatially filtered and recollimated to final diameters of ~0.4 cm. Portions of these beams were diverted to photodiode assemblies that measured the energies of individual pulses, thereby enabling active (shot-by-shot) normalization of TC-RFWM signals [as per the $I_1I_2I_3 \equiv I_{\mathrm{PUMP}}(I_{\mathrm{DUMP}})^2$ scaling of eq 22] designed to mitigate the effects of power fluctuations and long-term drift. External triggering of the two Nd:YAG lasers ensured temporal overlap of incoming electromagnetic fields at the sample interaction region.

Consistent with the SEP process outlined in Figure 1, the DUMP was separated into two beams of roughly equal intensities by means of an achromatic beamsplitter. The resulting PUMP ($\mathbf{E}_1$) and DUMP ($\mathbf{E}_2$ and $\mathbf{E}_3$) input waves were directed along three distinct major diagonals of a rectangular parallelepiped (~1.1° crossing angle), with their region of mutual intersection (viz., the RFWM interaction volume) located in the center of a stainless-steel vacuum chamber. The linear-polarization contrast ratio for each impinging field was enhanced by propagating through high-quality calcite Glan-Laser prisms (Karl Lambrecht Corp.) just prior to entering this sample vessel, where carefully mounted fused-silica windows minimized the deleterious effects of stress-induced birefringence.[10,11] Ancillary optical components (e.g., Fresnel Rhombs) inserted into beam paths allowed any fixed combination of $\boldsymbol{\varepsilon}_1$, $\boldsymbol{\varepsilon}_2$, and $\boldsymbol{\varepsilon}_3$ (all linearly polarized) to be established during a given experiment; however, the detected direction of linear polarization, $\boldsymbol{\varepsilon}_4$, was made adjustable by having the signal wave ($\mathbf{E}_4$) pass through a rotatable calcite-prism analyzer that was situated immediately after the target medium.

The polarization-resolved TC-RFWM signal photons emerging from the interaction region were isolated and sent through both spectral and spatial filters before impinging upon a high-speed photomultiplier assembly (Hamamatsu R7400P-03). The resulting photocurrent was amplified and directed to a CAMAC-based gated charge integrator (LeCroy 2249SG with Stanford Research Systems DG535 gate generator) that enabled the four-wave mixing amplitude, as well as related frequency and intensity metrics, to be recorded as a function of DUMP wavelength. Spectra typically were obtained by averaging the response produced by 128 shots of the Nd:YAG systems for each ~0.006 cm^{-1} increment of the DUMP frequency, with unfocused energies of ~300 nJ/pulse and ~7.5 μJ/pulse being employed for the PUMP and the DUMP, respectively, so as to minimize optical saturation effects (which are not expected to affect polarization-based suppression schemes strongly).[10,11] All data acquisition and laser tuning tasks were controlled by a dedicated personal computer running a custom LabView software package. The fixed frequency needed to access a specific PUMP transition for the SEP implementation of TC-RFWM (cf., Figure 1) was selected by performing one-color four-wave mixing (DFWM) measurements on tropolone samples prior to introduction of the DUMP light.[10,11] This process was facilitated by kinematically mounted optical components (not shown in Figure 2) that could be inserted reproducibly into the path of the PUMP beam to establish requisite phase-matching and signal-detection geometries for polarized forward-box DFWM spectroscopy.

Tropolone was obtained commercially (Aldrich Chemical Co.; 98% stated purity) and used without further purification. During experiments, crystalline tropolone was placed in a jacketed glass vessel kept at 25 °C by means of a thermostatted water bath. This apparatus incorporated a Teflon vacuum stopcock and O-ring flange that allowed it to be connected directly to the stainless-steel TC-RFWM chamber, which, in turn, was evacuated by a liquid-nitrogen-baffled diffusion pump. A steady flow of tropolone vapor through the interaction region was achieved by opening the stopcock of the sample vessel and regulating the pumping speed of the vacuum system while monitoring a capacitance manometer (MKS Baratron 122A) to maintain a constant internal pressure of ≤10 mTorr. When not in use, tropolone was stored *in vacuo* to minimize its degradation.

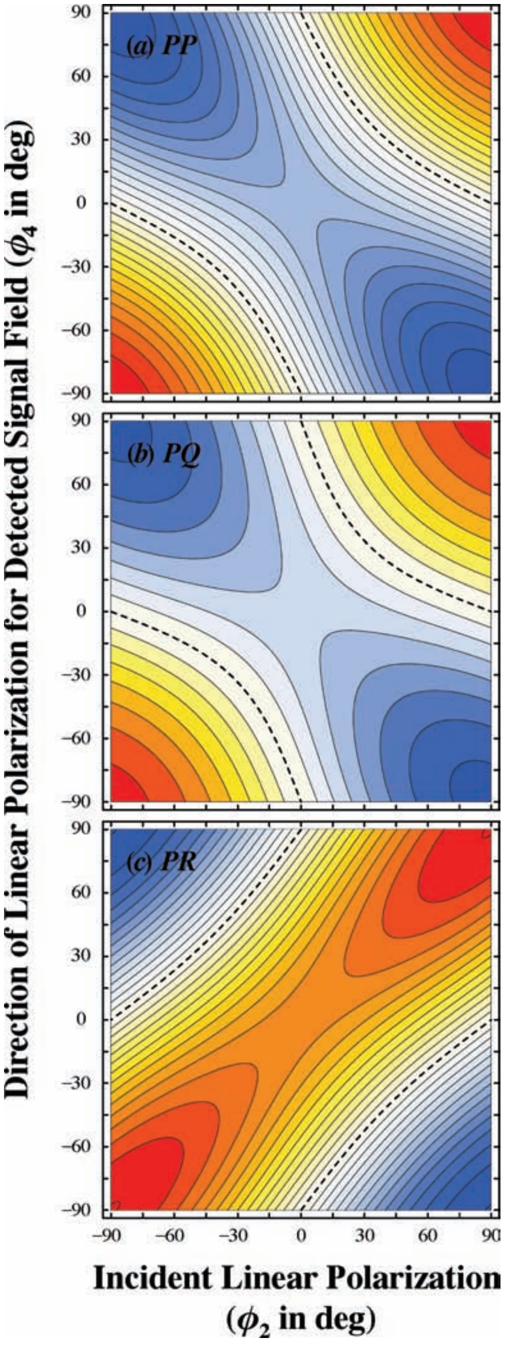

Figure 3. Contour plots of TC-RFWM response. The isotropic (rank-zero) element of the scaled TC-RFWM response tensor for the $\phi_4 Y \phi_2 Y$ polarization geometry is mapped as a function of angles ϕ_2 and ϕ_4 by using successive contour levels of 0.01 magnitude. A *P*-branch PUMP line is assumed, with the behavior predicted for (a) *P*-type (−0.137, −0.068, +0.137), (b) *Q*-type (−0.074, −0.028, +0.074), and (c) *R*-type (−0.140, +0.105, +0.140) DUMP transitions displayed separately, where numbers in parentheses denote values of $(2J_g + 1)^{3/2}\ R_0^{(0)}(\phi_4 Y \phi_2 Y; J_g, J_e, J_h, J_e)$ calculated at the (ϕ_2, ϕ_4) coordinates of (∓90°, ±90°), (0°, 0°), and (±90°, ±90°), respectively. The dashed contours found in each panel distinguish the loci of points where the response tensor is expected to vanish, thereby leading to suppression of the associated SEP spectral features.

IV. Results and Discussion

The branch-suppression schemes discussed in this paper rely upon the fact that the isotropic (rank-zero) TC-RFWM response tensor, $R_0^{(0)}(\boldsymbol{\varepsilon}_4^*\boldsymbol{\varepsilon}_3\boldsymbol{\varepsilon}_2^*\boldsymbol{\varepsilon}_1;J_g,J_e,J_h,J_f)$, can be made to vanish for certain combinations of incident/detected polarizations ($\boldsymbol{\varepsilon}_4^*\boldsymbol{\varepsilon}_3\boldsymbol{\varepsilon}_2^*\boldsymbol{\varepsilon}_1$) and PUMP/DUMP transitions (ΔJ_{eg}, ΔJ_{eh}, ΔJ_{fh}). These characteristics are described independently by the cosine functions and expansion coefficients of eq 23, with the angular arguments of the former quantities specifying a given arrangement of linear-polarized fields. Although not essential for the SEP processes addressed here, it proves convenient to consider a simplified $\phi_4\vartheta\phi_2\vartheta$ geometry where $\boldsymbol{\varepsilon}_1$ and $\boldsymbol{\varepsilon}_3$ are directed along a common axis given by $\phi_1 = \phi_3 = \vartheta$. The ensuing analyses also will assume that pertinent matter-field interactions are driven by an isolated pair of PUMP and DUMP lines, with $\eta_f = \eta_e$ and $J_f = J_e$, such that $|f\rangle$ and $|e\rangle$ represent degenerate eigenstates belonging to the same intermediate level (cf., Figure 1). Under such circumstances, ΔJ_{eg} and $\Delta J_{eh} = \Delta J_{fh}$ can be equated to the changes in rotational angular momentum induced by the PUMP and DUMP transitions, respectively.

Despite the simplifications outlined above, the TC-RFWM signal intensity still depends on three polarization angles (ϑ, ϕ_2, ϕ_4) and three angular momentum quantum numbers (J_g, J_e, J_h), where the latter can be expressed in terms of J_g by specifying the nature of the PUMP ($\Delta J_{eg} = J_e - J_g$) and the DUMP ($\Delta J_{eh} = J_e - J_h$) resonances. Figure 3 presents contour diagrams obtained by plotting the scaled response tensor of eq 23 as a function of ϕ_2 and ϕ_4 under the assumption of $\vartheta = \pi/2$, which implies a $\phi_4 Y\phi_2 Y$ geometry having $\boldsymbol{\varepsilon}_1$ and $\boldsymbol{\varepsilon}_3$ directed along the Y-axis (cf., eq 3). These results were computed for a P-branch PUMP line ($\Delta J_{eg} = -1$) having $J_g = 20$, with the three panels reflecting the unique properties obtained for (a) P-type ($\Delta J_{eh} = -1$), (b) Q-type ($\Delta J_{eh} = 0$), and (c) R-type ($\Delta J_{eh} = +1$) DUMP transitions. Since SEP studies of vibrationally excited molecules typically fix the PUMP frequency while the DUMP frequency is scanned, the spectroscopic utility of our branch-suppression methodology depends critically on the differences that exist between the doubly resonant *PP*, *PQ*, and *PR* processes of Figure 3. Even a cursory inspection shows that the behavior predicted for *PR* is distinct from those found for *PP* and *PQ*, thereby suggesting that the former can be distinguished from the latter through use of a $\phi_4 Y\phi_2 Y$ polarization scheme.

Of special consequence for the present work are the dashed contours in Figure 3, which highlight the loci of correlated (ϕ_2, ϕ_4) points that cause the scaled TC-RFWM response tensor and attendant SEP signal intensity to vanish. Similar two-dimensional analyses can be performed for other choices of J_g and ΔJ_{eg}; however, it proves more informative to fix the transverse characteristics for the remaining incident field (ϕ_2) and subsequently determine the direction of linear polarization that must be detected (ϕ_4) to eliminate a particular subset of doubly resonant features. Figure 4 displays results obtained for the practically convenient case of $\phi_2 = \pi/4$ (or 45°), with the three panels distinguishing the behavior obtained by implementing this $\phi_4 Y45°Y$ geometry through use of (a) P-branch ($\Delta J_{eg} = -1$), (b) Q-branch ($\Delta J_{eg} = 0$), and (c) R-branch ($\Delta J_{eg} = +1$) PUMP lines. In each panel, the value of ϕ_4 required to suppress P-type, Q-type, and R-type DUMP resonances is plotted as a function of the initial angular momentum quantum number, J_g, reflecting the implicit dependence of eq 23 on this quantity.

The ordinate scales in Figure 4 display the direction of signal linear polarization (ϕ_4) that must be detected to eliminate specific rotational transitions from TC-RFWM spectra recorded in the $\phi_4 Y45°Y$ geometry. For low quantum numbers, such suppression-inducing angles are predicted to change markedly between adjacent J_g values; however, the requisite ϕ_4 parameters clearly approach high$-J_g$ asymptotes that depend on the branch structure of the doubly resonant SEP process (ΔJ_{eg} and ΔJ_{eh}) but are independent of J_g. This behavior can be quantified by considering the $J_g \to \infty$ limit of the scaled rank-zero response tensor:

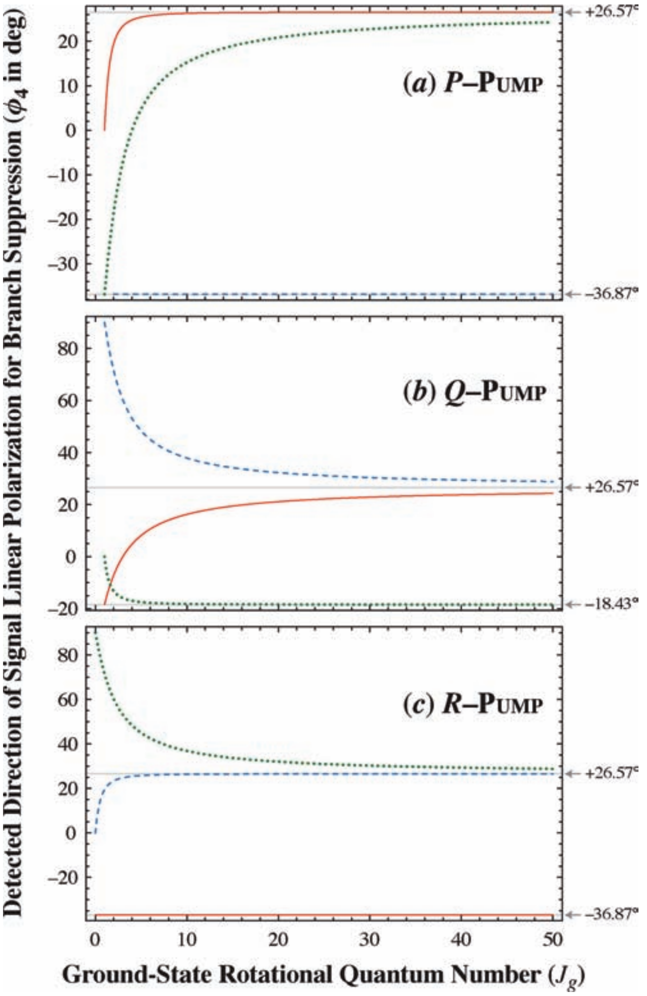

Figure 4. Angular momentum dependence of branch-suppression angles. The detected direction of linear polarization (ϕ_4) required to eliminate P-type (solid curve), Q-type (dotted curve), and R-type (dashed curve) DUMP resonances is plotted as a function of ground-state angular momentum quantum number (J_g), with separate panels showing the behavior predicted for (a) P-branch, (b) Q-branch, and (c) R-branch PUMP transitions. These results were obtained for a collinear implementation of the prototypical $\phi_4 Y45°Y$ polarization configuration. Rapid variations in ϕ_4 are observed for low values of J_g; however, asymptotic limits (cf., horizontal gray bars and attendant labels) are approached as J_g increases.

$$\lim_{J_g\to\infty}[(2J_g + 1)^{3/2}R_0^{(0)}(\phi_4\phi_3\phi_2\phi_1;J_g,J_e,J_h,J_e)] = \frac{1}{60}[A\cos(\phi_1 + \phi_2 - \phi_3 - \phi_4) + B\cos(\phi_1 - \phi_2 + \phi_3 - \phi_4) + C\cos(\phi_1 - \phi_2 - \phi_3 + \phi_4)] \quad (24)$$

with the purely numerical constant preceding each cosine function being the limiting value of the analogous coefficient ratio from eq 23. In particular, *A*, *B*, and *C* can be defined in terms of the angular momentum changes for the `PUMP` (ΔJ_{eg}) and the `DUMP` (ΔJ_{eh}) transitions:

$$A = 4 - \frac{3}{2}\left|\Delta J_{eg}\right| - \frac{3}{2}\left|\Delta J_{eh}\right| + \frac{1}{2}\left(1 + 4\left|\Delta J_{eg}\right|\left|\Delta J_{eh}\right|\right)\left|\Delta J_{hg}\right| \tag{25}$$

$$B = 4 + \left|\Delta J_{eg}\right| + \left|\Delta J_{eh}\right| - \frac{1}{2}\left(4 + \left|\Delta J_{eg}\right|\left|\Delta J_{eh}\right|\right)\left|\Delta J_{hg}\right| \tag{26}$$

$$C = 4 - \frac{3}{2}\left|\Delta J_{eg}\right| - \frac{3}{2}\left|\Delta J_{eh}\right| - \frac{9}{2}\left(1 - \left|\Delta J_{eg}\right|\left|\Delta J_{eh}\right|\right)\left|\Delta J_{hg}\right| \tag{27}$$

where $\Delta J_{hg} = J_h - J_g = \Delta J_{eg} - \Delta J_{eh}$. These high$-J_g$ constants are compiled in Table 6, along with analogous quantities derived for the more general case of $\Delta J_{fh} \neq \Delta J_{eh}$.

Figure 5 contains plots of eq 24 as a function of ϕ_4 for the aforementioned $\phi_4 Y45°Y$ geometry (i.e., $\phi_1 = \phi_3 = \pi/2$ and $\phi_2 = \pi/4$). Each panel displays the results obtained for a given type of `PUMP` line ($\Delta J_{eg} = -1$, 0, or $+1$), with the accompanying curves distinguishing the dependence predicted for the three possible classes of `DUMP` transitions ($\Delta J_{eh} = -1$, 0, or $+1$). In every case, the high$-J_g$ limit of the scaled TC-RFWM response tensor is found to cross the zero-line of the ordinate scale at a single value of ϕ_4, implying that suppression of the attendant SEP intensity can be realized by arranging for selective detection of this signal polarization, $\phi_{4,\{\Delta J_{eg}\}\{\Delta J_{eh}\}}$, where the symbols $\{\Delta J_{eg}\}$ and $\{\Delta J_{eh}\}$ can separately assume the designations "*P*", "*Q*", or "*R*". The symmetry of the $\phi_4 Y45°Y$ configuration permits only one `DUMP` rotational branch to be eliminated independently from the other two (e.g., $\phi_{4,PR} \neq \phi_{4,PP/PQ}$, where $\phi_{4,PP/PQ} = \phi_{4,PP} = \phi_{4,PQ}$); however, complete spectral discrimination is facilitated by the fact that the identity of this unique `DUMP` feature changes with the nature of the `PUMP` resonance.

As demonstrated by Figures 4 and 5, the direction of linear signal polarization required to suppress a given subset of doubly resonant SEP features follows from the roots of the pertinent TC-RFWM response tensor element. Given the asymptotic properties exhibited by such quantities, a straightforward analysis performed in the high$-J_g$ limit of eq 24 shows that:

$$\tan\phi_4 = -\frac{A\cos(\phi_1+\phi_2-\phi_3) + B\cos(\phi_1-\phi_2+\phi_3) + C\cos(\phi_1-\phi_2-\phi_3)}{A\sin(\phi_1+\phi_2-\phi_3) + B\sin(\phi_1-\phi_2+\phi_3) - C\sin(\phi_1-\phi_2-\phi_3)} \xrightarrow{\phi_1=\phi_3=\vartheta} -\frac{(A+C)\cos\phi_2 + B\cos(2\vartheta-\phi_2)}{(A+C)\sin\phi_2 + B\sin(2\vartheta-\phi_2)} \xrightarrow{\vartheta=\pi/2,\,\phi_2=\pi/4} -\frac{A-B+C}{A+B+C} \tag{28}$$

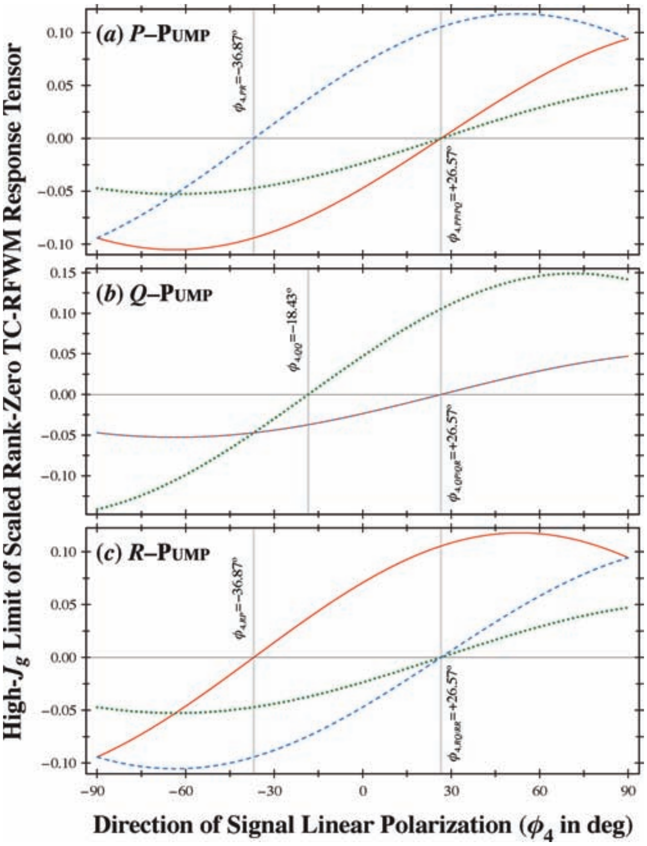

Figure 5. Asymptotic TC-RFWM branch suppression. The high$-J_g$ limit of the scaled (rank-zero) TC-RFWM response tensor is plotted as a function of the linear polarization angle detected for the signal field (ϕ_4) under the assumption of a collinear $\phi_4 Y45°Y$ geometry. The three panels highlight predictions obtained for (a) *P*-branch, (b) *Q*-branch, and (c) *R*-branch `PUMP` transitions, with the distinct behavior engendered by meshing *P*-type, *Q*-type, and *R*-type `DUMP` resonances being distinguished by solid, dotted, and dashed lines, respectively. Selective branch-suppression conditions are expected to exist whenever one of the displayed curves crosses the zero-line of the ordinate scale, as denoted by superimposed vertical gray bars and accompanying values of $\phi_{4,\{\Delta J_{eg}\}\{\Delta J_{eh}\}}$.

where the final two equalities follow first from assuming that both $\mathbf{E}_1$ and $\mathbf{E}_3$ are linearly polarized along a common axis (ϕ_1

TABLE 2: TC-RFWM Branch-Suppression Angles[a]

transition designation			signal polarization for transition suppression	
label	ΔJ_{eg}	ΔJ_{eh}	angle label	value for $\phi_4 Y45°Y$ geometry
PP	−1	−1	$\phi_{4,PP}$	$\tan^{-1}(1/2) \approx +26.57°$
PQ	−1	0	$\phi_{4,PQ}$	$\tan^{-1}(1/2) \approx +26.57°$
PR	−1	+1	$\phi_{4,PR}$	$\tan^{-1}(-3/4) \approx -36.87°$
QP	0	−1	$\phi_{4,QP}$	$\tan^{-1}(1/2) \approx +26.57°$
QQ	0	0	$\phi_{4,QQ}$	$\tan^{-1}(-1/3) \approx -18.43°$
QR	0	+1	$\phi_{4,QR}$	$\tan^{-1}(1/2) \approx +26.57°$
RP	+1	−1	$\phi_{4,RP}$	$\tan^{-1}(-3/4) \approx -36.87°$
RQ	+1	0	$\phi_{4,RQ}$	$\tan^{-1}(1/2) \approx +26.57°$
RR	+1	+1	$\phi_{4,RR}$	$\tan^{-1}(1/2) \approx +26.57°$

[a] The directions of signal polarization (ϕ_4) that must be detected to cause specific subsets of SEP resonances to be suppressed in the $\phi_4 Y45°Y$ configuration are presented, with results being partitioned according to the angular momentum changes induced by the `PUMP` (ΔJ_{eg}) and the `DUMP` (ΔJ_{eh}) transitions. Tabulated polarization angles follow from roots of the scaled (rank-zero) TC-RFWM response tensor, as evaluated under asymptotic high$-J_g$ limiting conditions.

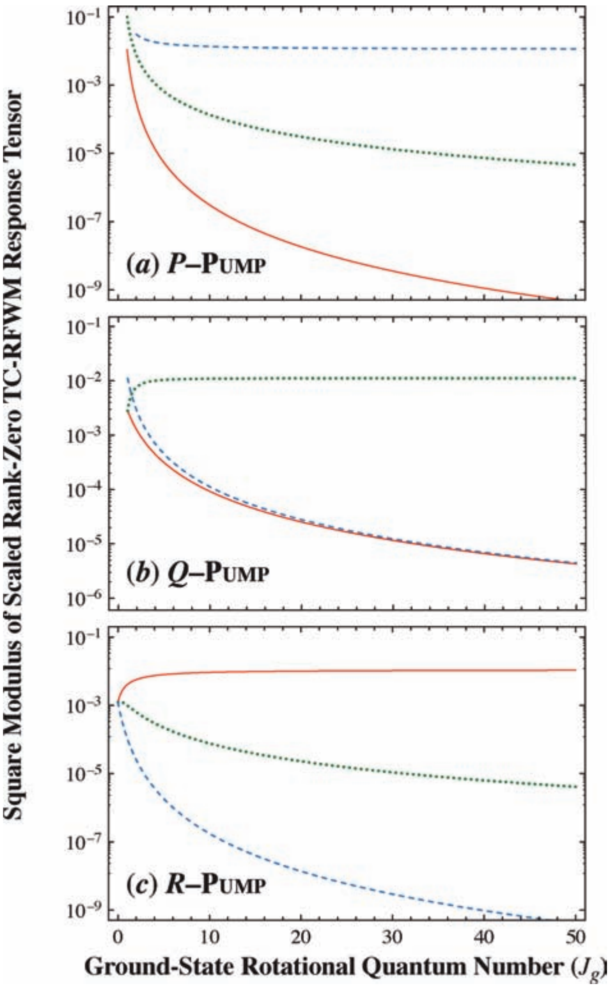

Figure 6. Influence of asymptotic TC-RFWM branch-suppression angles. The square modulus of the scaled isotropic (rank-zero) TC-RFWM response tensor is plotted as a function of ground-state angular momentum quantum number (J_g) with *P*-type, *Q*-type, and *R*-type DUMP transitions being distinguished through use of solid, dotted, and dashed curves, respectively. The three panels highlight behavior predicted for (a) *P*-branch, (b) *Q*-branch, and (c) *R*-branch PUMP lines in the $\phi_4 Y45°Y$ polarization configuration, where ϕ_4 has been fixed at $\tan^{-1}(1/2) \approx +26.57°$ to examine DUMP resonances having suppression angles that converge slowly to their asymptotic high$-J_g$ limits. As J_g increases, a precipitous drop in $|(2J_g + 1)^{3/2}R_0^{(0)}(\phi_4 Y45°Y; J_g, J_e, J_h, J_e)|^2$ is expected for the targeted SEP features, implying that a corresponding reduction in relative TC-RFWM signal intensity should be realized.

$= \phi_2 = \vartheta$) and second by adopting the $\phi_4 Y45°Y$ geometry ($\vartheta = \pi/2$ and $\phi_2 = \pi/4$). Table 2 contains a compilation of suppression angles derived for the latter case, with the tabulated numerical values of $\phi_{4,\{\Delta J_{eg}\}\{\Delta J_{eh}\}}$ partitioned according to the changes in angular momentum incurred by allowed PUMP and DUMP transitions. Aside from the previously mentioned ability to isolate only a single DUMP branch for a given choice of PUMP line, the symmetry of the $\phi_4 Y45°Y$ scheme leads to $\phi_{4,\{\Delta J_{eg}\}\{\Delta J_{eh}\}} = \phi_{4,\{\Delta J_{eh}\}\{\Delta J_{eg}\}}$, implying, for example, that the detector polarization needed to eliminate *R*-type DUMP features induced by a *P*-branch PUMP ($\phi_{4,PR}$) is the same as that required to suppress *P*-type DUMP resonances recorded with an *R*-branch PUMP ($\phi_{4,RP}$). Such constraints do not affect more general TC-RFWM polarization configurations, where independent selection of transverse characteristics for the three incident electromagnetic waves ($\boldsymbol{\varepsilon}_1 \neq \boldsymbol{\varepsilon}_2 \neq \boldsymbol{\varepsilon}_3$) can enable any desired family of branch-resolved features to be removed selectively from the SEP spectrum.

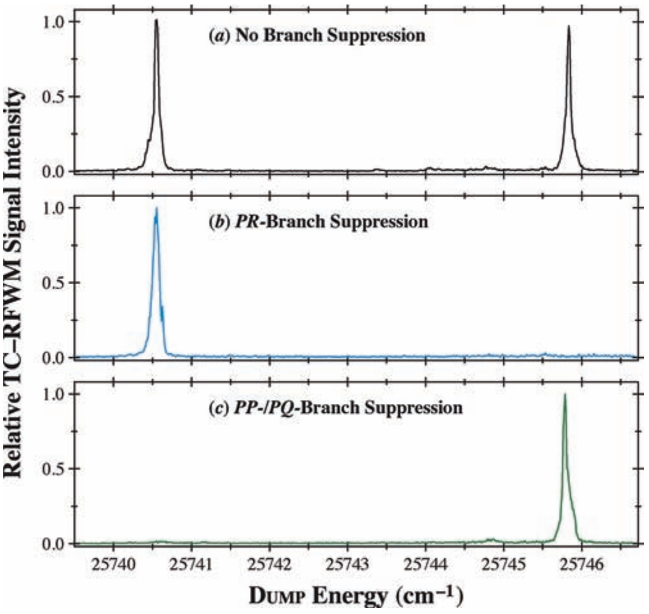

Figure 7. Experimental verification of TC-RFWM branch suppression. The symmetric member of the tunneling-split $v_{15} = 1$ vibrational level in the ground electronic state of tropolone was probed under ambient, bulk-gas conditions by exploiting an isolated *P*-branch PUMP feature in the 0_0^+ origin band of the $\tilde{A}-\tilde{X}$ absorption system that arises primarily from the $^{b,R}P_0(38)$ and $^{b,P}P_1(38)$ lines. The depicted SEP data were acquired through use of the $\phi_4 Y45°Y$ configuration with the direction of linear polarization detected for the generated TC-RFWM signal field (ϕ_4) set equal to (a) $\phi_4 = \pi/2$, (b) $\phi_{4,PR} = -36.87°$, and (c) $\phi_{4,PQ/PR} = +26.57°$, where the latter two arrangements lead to the selective suppression of *R*-type and combined *P*-/*Q*-type DUMP transitions, respectively.

For a given PUMP line, the $\phi_4 Y45°Y$ results of Figure 4 show that the suppression angle for one DUMP branch reaches its high$-J_g$ limit rapidly while those for the other two require substantially larger angular momentum quantum numbers to approach their common asymptote. This behavior would appear to compromise the utility of our polarization-based methodology, suggesting that the ϕ_4 parameter needed to quench a particular subset of SEP features will depend strongly on J_g. Arguments to the contrary can be found in Figure 6, where relative magnitudes of $I_4(\omega)$ (cf., eq 22) are gauged by plotting the square modulus of the scaled TC-RFWM response tensor, $|(2J_g + 1)^{3/2} R_0^{(0)}(\phi_4 Y45°Y; J_g, J_e, J_h, J_e)|^2$, as a function of J_g. For this analysis, the detected direction of linear polarization has been set equal to the asymptotic value predicted for the pair of slowly converging DUMP branches (viz., $\phi_4 = +26.57°$) accessed by (a) *P*-type, (b) *Q*-type, and (c) *R*-type PUMP transitions. The logarithmic nature of the ordinate scale in each panel serves to highlight the dramatic falloff in signal strength expected for suppressed branches as J_g increases, showing that over a 100-fold reduction in intensity (relative to that of unsuppressed branches) can be attained by $J_g = 10$. As such, the $\phi_4 Y45°Y$ configurations summarized in Table 2 should afford a robust means for simplifying and interpreting complex spectral patterns. In practice, forward-box phase-matching geometries of high aspect ratio (i.e., involving small crossing angles) should incur negligible deviations from the collinear assumptions employed for the present calculations, with the fixing of incident and detected polarization angles to within ±1° being sufficient to realize the desired suppression properties.

Figure 7 presents a graphical illustration of TC-RFWM branch-suppression schemes as applied to tropolone, a prototypical proton-transfer system in which an intramolecular hydrogen bond adjoins hydroxylic (proton-donating) and ketonic (proton-accepting) oxygen centers.[43] Both the ground ($\tilde{X}^1A_1$) and the first-excited singlet ($\tilde{A}^1B_2$) electronic states of this molecule support symmetric, double-minimum wells along the O···H···O reaction coordinate,[12,44] with a potential barrier of finite height separating two stable enol tautomers of planar geometry. Although classically hindered, rapid interconversion between these equivalent conformers can occur by means of quantum-mechanical (proton) tunneling, thereby leading to a characteristic bifurcation of all rovibronic features into symmetric (+) and antisymmetric (−) components (with respect to the proton-transfer coordinate). The magnitude of this splitting, which scales in proportion to the rate of hydron migration, is affected strongly by the redistribution of charge density and the displacement of heavy nuclei that accompanies electronic[11] and/or vibrational[13] excitation. Consequently, spectroscopic measurement of such tunneling-induced signatures can provide a direct probe for the multidimensional nature of the underlying proton-transfer dynamics.[43]

The data in Figure 7 were acquired under ambient, bulk-gas conditions by fixing the PUMP energy at 27014.62 cm^{-1} so as to excite a specific *P*-branch feature within the 0^{+}_{+} origin band of the tropolone $\tilde{A}^1B_2$−$\tilde{X}^1A_1$ ($\pi^* \leftarrow \pi$) absorption system. As documented by our prior DFWM studies,[11] this selection accesses a cluster of closely spaced rovibronic lines dominated by ${}^{b,R}P_0(38)$ and ${}^{b,P}P_1(38)$, but also including other members of the ${}^{b,R}P_{K_a}(J)$ and ${}^{b,P}P_{K_a}(J)$ families ($J \leq 38$), where $J + K_a$ equals 38 and 39, respectively. Scanning of the DUMP laser in the vicinity of 25745 cm^{-1} reveals pronounced TC-RFWM signals that can be attributed to rotational structure arising from the symmetric (+) component of the 15^0_1 transition (viz., 15^{0+}_{1+}), where ν_{15} corresponds to an in-plane mode of a_1 character (as classified in the encompassing G_4 permutation-inversion group) that entails substantial C−H/O−H wagging and C=O stretching motions.[12] The rotationless $v_{15} = 1$ level is found to reside 1274.1 cm^{-1} above the zero-point energy of the ground electronic state, a result in reasonable accord with the harmonic prediction of 1307.2 cm^{-1} from high-level *ab initio* calculations.[12] A detailed analysis of this vibrational manifold will be reported elsewhere; however, the attendant displacement of the nuclear framework serves to enhance the rate of proton transfer markedly, with the tunneling-induced bifurcation measured for $v_{15} = 1$ exceeding that of its vibrationless ($v = 0$) counterpart by more than a factor of two.

The three tropolone data sets of Figure 7 were obtained sequentially by changing the direction of linear polarization detected for the signal field emerging from a nearly collinear (forward-box) implementation of the $\phi_4Y45°Y$ polarization scheme. The topmost panel depicts results obtained by setting $\phi_4 = \pi/2$ (*Y*-polarized), an arrangement designed to mimic the canonical *YYYY* configuration which maximizes the four-wave mixing response evoked from an isotropic medium.[27,37] Two intense peaks attributable to the 15^{0+}_{1+} DUMP resonance dominate this trace, with their narrow widths reflecting the small differences in rotational constants that must exist between the initial ($v = 0$) and targeted ($v_{15} = 1$) vibrational manifolds of the ground electronic state. Quantitative spectral simulations based on the weak-field TC-RFWM formalism of Section II confirm that the pronounced features located at 25740.53 and 25745.75 cm^{-1}, respectively, arise from overlapping *P*-branch ($\Delta J_{eh} = -1$) and *R*-branch ($\Delta J_{eh} = +1$) rotational structure within the 15^{0+}_{1+} band. Such analyses also predict *Q*-branch ($\Delta J_{eh} = 0$) DUMP transitions to be substantially weaker than their *P*-branch and *R*-branch analogues, thus causing them to be obscured by baseline fluctuations.

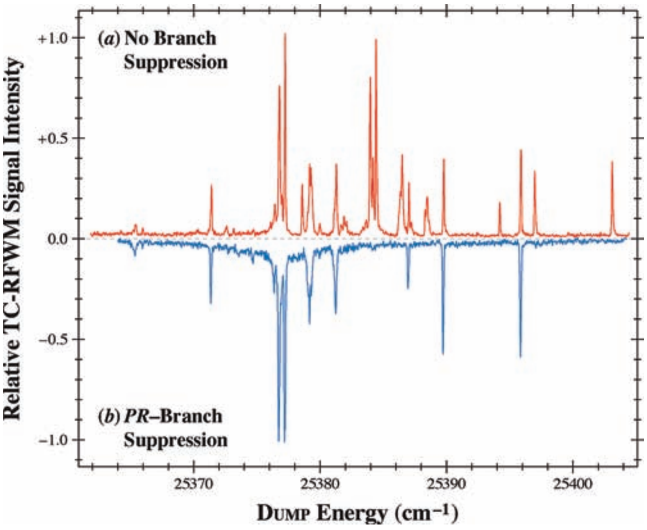

Figure 8. TC-RFWM branch suppression for complex SEP spectra. An isolated *P*-branch PUMP feature in the 0^{+}_{+} origin band of the tropolone $\tilde{A}$−$\tilde{X}$ absorption system attributed primarily to the ${}^{b,R}P_0(53)$ and ${}^{b,P}P_1(53)$ lines was used to explore ground-state vibrational levels having rotationless energies that span the 1610−1650 cm^{-1} range. Two TC-RFWM spectra are displayed, one (upper trace) acquired in the *YYYY* polarization configuration that permits all DUMP features to be observed and the other (lower trace; inverted for ease of comparison) recorded though use of the $\phi_4Y45°Y$ branch-suppression scheme with the direction of linear polarization detected for the generated signal field (ϕ_4) being set equal to $\phi_{4,PR} = -36.87°$ so as to eliminate *R*-type DUMP resonances.

The lower panels in Figure 7 display the TC-RFWM response obtained by setting (b) $\phi_4 = -36.87°$ and (c) $\phi_4 = +26.57°$, thereby establishing the polarization configurations needed to suppress *R*-branch ($\phi_{4,PR}$) and *P*-/*Q*-branch ($\phi_{4,PP/PQ}$) DUMP transitions, respectively, for a *P*-branch PUMP line ($\Delta J_{eg} = -1$). The pronounced peak residing at 25745.75 cm^{-1} in the *YY*45°*Y* trace vanishes from the middle panel, thus confirming the *R*-type character of this feature. Similarly, the strong *YY*45°*Y* signal at 25740.53 cm^{-1} is absent from the bottom panel, in keeping with its *P*-type assignment. The small resonances barely discernible from baseline noise in these SEP spectra are believed to arise from interloping $\tilde{X}^1A_1$ vibrational levels.

While the results in Figure 7 corroborate the theoretical framework outlined in Section II, the practical utility of our polarization-based detection schemes can be appreciated best by examining higher-lying portions of the $\tilde{X}^1A_1$ potential surface, where the mounting density of states eventually causes vibrational separations to become comparable to those of rotation-tunneling structure. An example of this situation can be found in Figure 8, which contrasts SEP spectra measured for tropolone with and without the benefits of branch suppression. These data were acquired by exciting an isolated *P*-branch feature in the $\tilde{A}$−$\tilde{X}$ origin band (0^{+}_{+}) at a fixed PUMP energy of 27013.17 cm^{-1}, thereby accessing a compact cluster of rovibronic transitions dominated by the ${}^{b,R}P_0(53)$ and ${}^{b,P}P_1(53)$ lines.[11] Scanning the DUMP laser over the range 25360−25410 cm^{-1} with the canonical *YYYY* polarization geometry (positive-going trace) reveals a significant number of intertwined vibronic resonances, each of which nominally contributes two strong peaks to the recorded pattern (cf., Figure 7a). Taking into account the rotational energy of observed $\tilde{X}^1A_1$ eigenstates, harmonic coupled-cluster calculations[12] predict three tropolone fundamentals to span the pertinent 1610−1650 cm^{-1} region above the zero-point level, $\nu_9(a_1)$ at 1638 cm^{-1}, $\nu_8(b_2)$ at 1694 cm^{-1}, and $\nu_7(a_1)$ at 1711 cm^{-1}, where only the latter two have been considered in band-contour analyses of high-resolution infrared absorption measurements.[45] In contrast, the spectral simplification inherent to the TC-RFWM technique permits many additional features to be resolved and suggests the possible onset of intramolecular vibrational redistribution (IVR) processes.[46]

The lower portion of Figure 8 depicts a TC-RFWM spectrum acquired for tropolone through use of the $\phi_4 Y45°Y$ polarization geometry, where ϕ_4 has been set equal to $\phi_{4,PR} = -36.87°$ so as to achieve R-branch `DUMP` suppression for a P-branch `PUMP` line. Even a cursory inspection of this trace, which has been inverted to facilitate comparison with its *YYYY* counterpart, demonstrates that essentially half of the SEP peaks have vanished. Assuming Q-branch structure to be weak (cf., Figure 7), features present in the $\phi_4 Y45°Y$ scan can be attributed primarily to P-branch `DUMP` resonances, while those displaced from the *YYYY* data set must stem from R-type transitions. Application of such branch-suppression schemes permits at least eight distinct vibrational levels to be identified over the targeted range of ground-state energies, with analogous results obtained by exciting the antisymmetric member of the $\tilde{A}-\tilde{X}$ origin band (0^-_-) enabling state-specific information to be extracted for the attendant dynamics of proton transfer. A detailed discussion of these and related tropolone measurements, including quantitative rotation-tunneling analyses of recorded spectral patterns, will be the subject of a forthcoming publication.

V. Summary and Conclusions

This paper has presented a synergistic theoretical and experimental investigation of stimulated emission pumping (SEP) processes as implemented within the coherent framework of two-color resonant four-wave mixing (TC-RFWM) spectroscopy. In particular, novel polarization geometries have been identified for the selective suppression of rovibronic features according to their attendant changes in rotational quantum numbers. Building upon the vector-recoupling formalism elaborated by our previous studies,[27] a third-order perturbative treatment of matter-field interactions has been combined with a state-multipole expansion of the unperturbed (zero-order) density operator to cast the weak-field signal intensity in terms of a TC-RFWM response tensor, $R_Q^{(K)}(\boldsymbol{\varepsilon}_4^*\boldsymbol{\varepsilon}_3\boldsymbol{\varepsilon}_2^*\boldsymbol{\varepsilon}_1;J_g,J_e,J_h,J_f)$. Of special importance are the intrinsic symmetry properties of the latter quantity, which enable the transverse characteristics for incident and generated electromagnetic waves ($\boldsymbol{\varepsilon}_4^*\boldsymbol{\varepsilon}_3\boldsymbol{\varepsilon}_2^*\boldsymbol{\varepsilon}_1$) to be effectively separated from the angular momentum properties of the participating `PUMP` and `DUMP` transitions (J_g,J_e,J_h,J_f). Since explicit assumptions have not been made regarding the distribution and correlation of probability amplitude among degenerate eigenstates composing the initial ground-state manifold, the resulting analyses afford a general solution for polarization-specific TC-RFWM behavior even in the presence of intrinsic angular momentum or rotational anisotropy (i.e., as described by molecular orientation and/or alignment parameters).[28,38,42]

For an isolated SEP process taking place in an isotropic ensemble of target molecules, only a single element of the response tensor needs to be considered, $R_0^{(0)}(\boldsymbol{\varepsilon}_4^*\boldsymbol{\varepsilon}_3\boldsymbol{\varepsilon}_2^*\boldsymbol{\varepsilon}_1;J_g,J_e,J_h,J_e)$, with its roots embodying the underlying criteria needed to discriminate against particular rovibronic features. By focusing on a collinear phase-matching geometry built upon linearly polarized electromagnetic waves and invoking the asymptotic behavior predicted for the limit of large quantum numbers ($J_g \rightarrow \infty$), judicious choice of the polarization angle detected for the TC-RFWM signal field was found to suppress `DUMP` resonances selectively according to the nature of their rotational branch (ΔJ_{eh}) and the rotational branch for the meshing `PUMP` line (ΔJ_{eg}). The feasibility and utility of this approach was demonstrated by performing polarization-resolved measurements on ambient tropolone vapor, where the fully allowed $\tilde{A}^1B_2-\tilde{X}^1A_1$ ($\pi^* \leftarrow \pi$) absorption system furnished the requisite `PUMP` and `DUMP` transitions. Two distinct regions of the $\tilde{X}^1A_1$ potential surface were explored, documenting the ability to selectively eliminate rotational structure through straightforward manipulation of optical polarization properties.

By combining the advantages of a background-free, absorption-based response with the selectivity inherent to a doubly resonant excitation process, the TC-RFWM implementation of SEP affords a powerful and robust tool for exploring ground-state potential surfaces systematically over wide swaths of internal energy. Unfortunately, the substantial number of vibrational modes and the small magnitude of rotational constants endemic to large polyatomic species routinely conspire to yield spectra of extraordinary complexity. Our branch-suppression techniques provide a viable means for resolving such rovibronic congestion, enabling intertwined features to be discriminated selectively while simultaneously facilitating their detailed assignment. The present work has focused on incident and generated electromagnetic waves of explicitly linear polarization; however, extension of the underlying formalism to more general transverse characteristics (e.g., circular or elliptical polarizations) should be straightforward and promises to introduce additional mechanisms for the efficient dissection of spectral patterns arising from rotationally anisotropic molecular distributions.[27] The methods outlined in this paper also should be applicable to other variants of TC-RFWM, including unfolded (e.g., hole-burning) schemes designed to unravel the structure and dynamics of electronically excited manifolds.

Acknowledgment. The work described in this paper was performed under the auspices of grant CHE-0809856 awarded by the Experimental Physical Chemistry Program in the Directorate for Mathematical and Physical Sciences of the United States National Science Foundation. One of the authors (L.A.B.) gratefully acknowledges the support of an NSF Graduate Research Fellowship.

Appendix

The TC-RFWM branch-suppression schemes introduced in this paper have focused primarily on an isolated SEP process involving a single intermediate manifold within the electronically excited potential surface (cf., Figure 1). Implicit to this description are the assumptions $\eta_f = \eta_e$ and $J_f = J_e$, with $|f\rangle$ and $|e\rangle$ relegated to degenerate eigenstates (i.e., magnetic sublevels) belonging to the same rovibronic energy level. It follows that the two `DUMP` transitions depicted in Figure 1 (induced by the ω_2 and ω_3 fields) are equivalent and belong to the same rotational branch ($\Delta J_{fh} = \Delta J_{eh}$). Similar considerations hold true for the meshing pair of `PUMP`

TABLE 3: Expansion Coefficients for TC-RFWM Response Tensor with *P*-Branch PUMP[a]

transition designation				coefficients for scaled rank-zero TC-RFWM response tensor				
label	ΔJ_{eg}	ΔJ_{eh}	ΔJ_{fh}	c_{00}	c_{12}	c_{13}	c_{14}	restriction
PPP	−1	−1	−1	$J_g(2J_g-1)$	$(J_g+1)(2J_g+3)$	$2(6J_g^2-1)$	$(J_g-1)(2J_g-3)$	$J_g \geq 1$
PPQ	−1	−1	0	J_g	$-(2J_g+3)$	$(3J_g+2)$	$3(J_g-1)$	$J_g \geq 1$
PPR	−1	−1	+1	1	1	1	6	$J_g \geq 1$
PQP	−1	0	−1	∅	∅	∅	∅	forbidden
PQQ	−1	0	0	$J_g(2J_g-1)$	$3(J_g+1)(2J_g+1)$	$(2J_g+1)(3J_g-2)$	$-(2J_g+1)(2J_g-3)$	$J_g \geq 1$
PQR	−1	0	+1	ξ_{PQR}	−3	2	−3	$J_g \geq 1$
PRP	−1	+1	−1	∅	∅	∅	∅	forbidden
PRQ	−1	+1	0	∅	∅	∅	∅	forbidden
PRR	−1	+1	+1	$(2J_g-1)$	$6(2J_g+1)$	$(2J_g+1)$	$(2J_g+1)$	$J_g \geq 2$

[a] The dimensionless expansion coefficients needed to describe the rank-zero element of the scaled TC-RFWM response tensor in eq 23 are tabulated as a function of initial rotational quantum number (J_g) for a *P*-branch PUMP line, with results being partitioned according to the angular momentum changes induced by DUMP transitions where ΔJ_{eh} and ΔJ_{fh} need not be equal.

$$\xi_{PQR} = J_g\sqrt{\frac{(2J_g - 1)}{(2J_g + 1)(J_g + 1)(J_g - 1)}}$$

TABLE 4: Expansion Coefficients for TC-RFWM Response Tensor with *Q*-Branch PUMP[a]

transition designation				coefficients for scaled rank-zero TC-RFWM response tensor				
label	ΔJ_{eg}	ΔJ_{eh}	ΔJ_{fh}	c_{00}	c_{12}	c_{13}	c_{14}	restriction
QPP	0	−1	−1	(J_g+1)	$3(J_g+2)$	$(3J_g+1)$	$-(2J_g-1)$	$J_g \geq 1$
QPQ	0	−1	0	ξ_{QPQ}	−3	2	−3	$J_g \geq 1$
QPR	0	−1	+1	∅	∅	∅	∅	forbidden
QQP	0	0	−1	J_g	$-(2J_g+3)$	$(3J_g+2)$	$3(J_g-1)$	$J_g \geq 1$
QQQ	0	0	0	$J_g(J_g+1)$	$4J_g(J_g+1)-3$	$4J_g(J_g+1)+2$	$4J_g(J_g+1)-3$	$J_g \geq 1$
QQR	0	0	+1	(J_g+1)	$-(2J_g-1)$	$(3J_g+1)$	$3(J_g+2)$	$J_g \geq 1$
QRP	0	+1	−1	∅	∅	∅	∅	forbidden
QRQ	0	+1	0	ξ_{QRQ}	−3	2	−3	$J_g \geq 1$
QRR	0	+1	+1	J_g	$3(J_g-1)$	$(3J_g+2)$	$-(2J_g+3)$	$J_g \geq 1$

[a] The dimensionless expansion coefficients needed to describe the rank-zero element of the scaled TC-RFWM response tensor in eq 23 are tabulated as a function of initial rotational quantum number (J_g) for a *Q*-branch PUMP line, with results being partitioned according to the angular momentum changes induced by DUMP transitions where ΔJ_{eh} and ΔJ_{fh} need not be equal.

$$\xi_{QPQ} = \frac{(2J_g + 3)(J_g + 1)}{\sqrt{J_g(J_g + 2)(2J_g + 1)(2J_g + 3)}}; \quad \xi_{QRQ} = J_g\sqrt{\frac{(2J_g - 1)}{(2J_g + 1)(J_g + 1)(J_g - 1)}}$$

TABLE 5: Expansion Coefficients for TC-RFWM Response Tensor with *R*-Branch PUMP[a]

transition designation				coefficients for scaled rank-zero TC-RFWM response tensor				
label	ΔJ_{eg}	ΔJ_{eh}	ΔJ_{fh}	c_{00}	c_{12}	c_{13}	c_{14}	restriction
RPP	+1	−1	−1	$(2J_g+3)$	$6(2J_g+1)$	$(2J_g+1)$	$(2J_g+1)$	
RPQ	+1	−1	0	∅	∅	∅	∅	forbidden
RPR	+1	−1	+1	∅	∅	∅	∅	forbidden
RQP	+1	0	−1	ξ_{RQP}	−3	2	−3	$J_g \geq 1$
RQQ	+1	0	0	$(J_g+1)(2J_g+3)$	$3J_g(2J_g+1)$	$(2J_g+1)(3J_g+5)$	$-(2J_g+1)(2J_g+5)$	
RQR	+1	0	+1	∅	∅	∅	∅	forbidden
RRP	+1	+1	−1	1	1	1	6	$J_g \geq 1$
RRQ	+1	+1	0	(J_g+1)	$-(2J_g-1)$	$(3J_g+1)$	$3(J_g+2)$	$J_g \geq 1$
RRR	+1	+1	+1	$(J_g+1)(2J_g+3)$	$J_g(2J_g-1)$	$12J_g(J_g+2)+10$	$(J_g+2)(2J_g+5)$	

[a] The dimensionless expansion coefficients needed to describe the rank-zero element of the scaled TC-RFWM response tensor in eq 23 are tabulated as a function of initial rotational quantum number (J_g) for an *R*-branch PUMP line, with results being partitioned according to the angular momentum changes induced by DUMP transitions where ΔJ_{eh} and ΔJ_{fh} need not be equal.

$$\xi_{RQP} = \frac{(2J_g + 3)(J_g + 1)}{\sqrt{J_g(J_g + 2)(2J_g + 1)(2J_g + 3)}}$$

TABLE 6: High−J_g Expansion Coefficients for Scaled TC-RFWM Response Tensor[a]

transition designation				high−J_g coefficients for TC-RFWM response tensor		
label	ΔJ_{eg}	ΔJ_{eh}	ΔJ_{fh}	A	B	C
PPP	−1	−1	−1	1	6	1
PPQ	−1	−1	0	−2	3	3
PPR	−1	−1	+1	1	1	6
PQP	−1	0	−1	∅	∅	∅
PQQ	−1	0	0	3	3	−2
PQR	−1	0	+1	−3	2	−3
PRP	−1	+1	−1	∅	∅	∅
PRQ	−1	+1	0	∅	∅	∅
PRR	−1	+1	+1	6	1	1
QPP	0	−1	−1	3	3	−2
QPQ	0	−1	0	−3	2	−3
QPR	0	−1	+1	∅	∅	∅
QQP	0	0	−1	−2	3	3
QQQ	0	0	0	4	4	4
QQR	0	0	+1	−2	3	3
QRP	0	+1	−1	∅	∅	∅
QRQ	0	+1	0	−3	2	−3
QRR	0	+1	+1	3	3	−2
RPP	+1	−1	−1	6	1	1
RPQ	+1	−1	0	∅	∅	∅
RPR	+1	−1	+1	∅	∅	∅
RQP	+1	0	−1	−3	2	−3
RQQ	+1	0	0	3	3	−2
RQR	+1	0	+1	∅	∅	∅
RRP	+1	+1	−1	1	1	6
RRQ	+1	+1	0	−2	3	3
RRR	+1	+1	+1	1	6	1

[a] The numerical coefficients needed to describe the rank-zero element for the scaled TC-RFWM response tensor as defined by the high−J_g limit of eq 24 are tabulated, with results being partitioned according to the angular momentum changes induced by the PUMP (ΔJ_{eg}) and the DUMP (ΔJ_{eh} and ΔJ_{fh}) transitions where ΔJ_{eh} and ΔJ_{fh} need not be equal.

resonances (induced by the ω_1 and ω_4 fields) and their branch labels ($\Delta J_{fg} = \Delta J_{eg}$).

The restrictions of the previous paragraph are not essential for a valid four-wave mixing pathway, where the most general circumstances entail $\eta_f \neq \eta_e$ and/or $J_f \neq J_e$ such that distinct pairs of PUMP ($\Delta J_{fg} \neq \Delta J_{eg}$) and DUMP ($\Delta J_{fh} \neq \Delta J_{eh}$) resonances exist. The underlying matter-field interactions still satisfy the conservation criteria imposed upon energy ($\omega_4 = \omega_1 - \omega_2 + \omega_3$) and momentum ($\mathbf{k}_4 = \mathbf{k}_1 - \mathbf{k}_2 + \mathbf{k}_3$); however, the resulting SEP process is more complicated, requiring juxtaposition of three branch labels, $\{\Delta J_{eg}\}\{\Delta J_{eh}\}\{\Delta J_{fh}\}$ (e.g., *PQR*), to fully specify its rotational character. Assuming that all incident and detected electromagnetic waves are polarized linearly along directions given by angles ϕ_j ($j = 1, 2, 3, 4$), the rank-zero element of the scaled TC-RFWM response tensor still can be defined by eq 23, with requisite expansion coefficients for each cosine function being compiled in Tables 3, 4, and 5 for the cases of *P*-branch, *Q*-branch, and *R*-branch PUMP lines (ΔJ_{eg}), respectively. The high−J_g limit of $(2J_g + 1)^{3/2}R_0^{(0)}(\phi_4\phi_3\phi_2\phi_1; J_g,J_e,J_h,J_f)$ can be cast in the same form as eq 24, where values for the numerical factors *A*, *B*, and *C* (which now depend on three quantities: ΔJ_{eg}, ΔJ_{eh}, and ΔJ_{fh}) can be found in Table 6. As before, viable branch-suppression strategies are encoded in the roots of the TC-RFWM response tensor, with the ancillary condition $\{\Delta J_{eh}\} \equiv \{\Delta J_{fh}\}$ leading to the basic schemes discussed in the text (e.g., $PQQ \equiv PQ$).

References and Notes

(1) Fischer, R. A. *Optical Phase Conjugation*; Academic Press, Inc.: San Diego, CA, 1983. Reintjes, J. F. *Nonlinear Optical Parametric Processes in Liquids and Gases*; Academic Press, Inc.: Orlando, FL, 1984.

(2) Wright, J. C.; Carlson, R. J.; Hurst, G. B.; Steehler, J. K.; Riebe, M. T.; Price, B. B.; Nguyen, D. C.; Lee, S. H. *Int. Rev. Phys. Chem.* **1991**, *10* (4), 349–390. Wright, J. C. *Int. Rev. Phys. Chem.* **2002**, *21* (2), 185–255.

(3) Mukamel, S. *Principles of Nonlinear Optical Spectroscopy*; Oxford University Press: New York, 1995. Butcher, P. N.; Cotter, D. *The Elements of Nonlinear Optics*; Cambridge University Press: Cambridge, U.K., 1990.

(4) Vaccaro, P. H. Degenerate Four-Wave Mixing (DFWM) Spectroscopy. In *Nonlinear Spectroscopy for Molecular Structure Determination*; Hirota, E., Field, R. W., Maier, J. P., Tsuchiya, S., Eds.; Blackwell Scientific Publications, Ltd.: London, 1998; Chapter 4, pp 75−126.

(5) Butenhoff, T. J.; Rohlfing, E. A. *J. Chem. Phys.* **1993**, *98* (7), 5460–5468.

(6) Arias, A. A.; Wasserman, T. A. W.; Vaccaro, P. H. *J. Chem. Phys.* **1997**, *107* (14), 5617–5620. Li, H.; Dupre, P.; Kong, W. *Chem. Phys. Lett.* **1997**, *273* (3,4), 272–278. Okazaki, A.; Ebata, T.; Mikami, N. *J. Chem. Phys.* **1997**, *107* (21), 8752–8758. Liu, C.-P.; Matsuda, Y.; Lee, Y.-P. *J. Chem. Phys.* **2003**, *119* (23), 12335–12341. Liu, C.-P.; Reid, S. A.; Lee, Y.-P. *J. Chem. Phys.* **2005**, *122* (12), 124313/1–8.

(7) Farrow, R. L.; Rakestraw, D. J. *Science* **1992**, *257* (5078), 1894–1900.

(8) Butenhoff, T. J.; Rohlfing, E. A. *J. Chem. Phys.* **1992**, *97* (2), 1595–1598.

(9) Müller, T.; Vaccaro, P. H. *Chem. Phys. Lett.* **1997**, *266* (5−6), 575–583.

(10) Bracamonte, A. E.; Vaccaro, P. H. *J. Chem. Phys.* **2003**, *119* (2), 887–901.

(11) Bracamonte, A. E.; Vaccaro, P. H. *J. Chem. Phys.* **2004**, *120* (10), 4658–4677.

(12) Burns, L. A.; Murdock, D.; Vaccaro, P. H. *J. Chem. Phys.* **2006**, *124* (20), 204307/1–15.

(13) Murdock, D.; Burns, L. A.; Vaccaro, P. H. *J. Chem. Phys.* **2007**, *127* (18), 181101/1–5.

(14) Kittrell, C.; Abramson, E.; Kinsey, J. L.; McDonald, S. A.; Reisner, D. E.; Field, R. W.; Katayama, D. H. *J. Chem. Phys.* **1981**, *75* (5), 2056–2059.

(15) Dai, H.-L.; Field, R. W. *Molecular Dynamics and Spectroscopy by Stimulated Emission Pumping*; World Scientific: Singapore, 1995.

(16) Kittrell, C. Stimulated Emission Pumping by Fluorescence Dip: Experimental Methods. In *Molecular Dynamics and Spectroscopy by Stimulated Emission Pumping*; Dai, H.-L., Field, R. W., Eds.; World Scientific: Singapore, 1995; Chapter 3, pp 109−147.

(17) Vaccaro, P. H.; Redington, R. L.; Schmidt, J.; Kinsey, J. L.; Field, R. W. *J. Chem. Phys.* **1985**, *82* (12), 5755–5756. Temps, F.; Halle, S.; Vaccaro, P. H.; Field, R. W.; Kinsey, J. L. *J. Chem. Phys.* **1987**, *87* (3), 1895–1897. Temps, F.; Halle, S.; Vaccaro, P. H.; Field, R. W.; Kinsey, J. L. *J. Chem. Soc., Faraday Trans. 2* **1988**, *84* (9), 1457–1482.

(18) Frye, D.; Liou, H. T.; Dai, H.-L. *Chem. Phys. Lett.* **1987**, *133* (3), 249–253. Vaccaro, P. H.; Temps, F.; Halle, S.; Kinsey, J. L.; Field, R. W. *J. Chem. Phys.* **1988**, *88* (8), 4819–4833.

(19) Moll, D. J.; Parker, G. R., Jr.; Kuppermann, A. *J. Chem. Phys.* **1984**, *80* (10), 4800–4807.

(20) Cooper, D. E.; Klimcak, C. M.; Wessel, J. E. *Phys. Rev. Lett.* **1981**, *46* (5), 324–328. Cooper, D. E.; Wessel, J. E. *J. Chem. Phys.* **1982**, *76* (5), 2155–2160. Suzuki, T.; Mikami, N.; Ito, M. *J. Phys. Chem.* **1986**, *90* (24), 6431–6440.

(21) Zhang, Q.; Kandel, S. A.; Wasserman, T. A. W.; Vaccaro, P. H. *J. Chem. Phys.* **1992**, *96* (2), 1640–1643.

(22) Vaccaro, P. H. Resonant Four-Wave Mixing Spectroscopy: A New Probe for Vibrationally-Excited Species. In *Molecular Dynamics and Spectroscopy by Stimulated Emission Pumping*; Dai, H.-L., Field, R. W., Eds.; World Scientific: Singapore, 1995; Chapter 1, pp 1−72.

(23) Buntine, M. A.; Chandler, D. W.; Hayden, C. C. *J. Chem. Phys.* **1992**, *97* (1), 707–710. Buntine, M. A.; Chandler, D. W.; Hayden, C. C. *J. Chem. Phys.* **1995**, *102* (7), 2718–2726.

(24) Butenhoff, T. J.; Rohlfing, E. A. *J. Chem. Phys.* **1993**, *98* (7), 5469–5476. Dunlop, J. R.; Rohlfing, E. A. *J. Chem. Phys.* **1994**, *100* (2), 856–862.

(25) Williams, S.; Tobiason, J. D.; Dunlop, J. R.; Rohlfing, E. A. *J. Chem. Phys.* **1995**, *102* (21), 8342–8358.

(26) Williams, S.; Rohlfing, E. A.; Rahn, L. A.; Zare, R. N. *J. Chem. Phys.* **1997**, *106* (8), 3090–3102.

(27) Wasserman, T. A. W.; Vaccaro, P. H.; Johnson, B. R. *J. Chem. Phys.* **1997**, *106* (15), 6314–6319. Wasserman, T. A. W.; Vaccaro, P. H.; Johnson, B. R. *J. Chem. Phys.* **1998**, *108* (18), 7713–7738. Müller, T.; Wasserman, T. A. W.; Vaccaro, P. H.; Johnson, B. R. *J. Chem. Phys.* **1998**, *108* (1), 4–7.

(28) Orr-Ewing, A. J.; Zare, R. N. *Annu. Rev. Phys. Chem.* **1994**, *45*, 315–366. Orr-Ewing, A. J.; Zare, R. N. *Adv. Ser. Phys. Chem.* **1995**, *6* (Chemical Dynamics and Kinetics of Small Radicals, Pt. 2), 936–1063.

(29) Hung, W.-C.; Huang, M.-L.; Lee, Y.-C.; Lee, Y.-P. *J. Chem. Phys.* **1995**, *103* (23), 9941–9946.

(30) Kumar, A.; Hsiao, C.-C.; Hung, W.-C.; Lee, Y.-P. *Chem. Phys. Lett.* **1997**, *269* (1,2), 22–28.

(31) McCormack, E. F.; Sarajlic, E. *Phys. Rev. A* **2001**, *63* (2), 023406/1–12.

(32) Chen, S.; Settersten, T. B. *Appl. Opt.* **2007**, *46* (19), 3911–3920.

(33) Costen, M. L.; McKendrick, K. G. *J. Chem. Phys.* **2005**, *112* (16), 164309/1–12.

(34) Wasserman, T. A. W.; Vaccaro, P. H.; Johnson, B. R. *J. Chem. Phys.* **2002**, *116* (23), 10099–10121.

(35) For the rarefied (gas-phase) media considered in the present study, the index of refraction is presumed to deviate insignificantly from that for a vacuum and to a good approximation one can set $n(\omega_j) \approx 1$. In a similar manner, correction factors for the local fields experienced by target molecules can justifiably be neglected.

(36) Oudar, J.-L.; Shen, Y. R. *Phys. Rev. A* **1980**, *22* (3), 1141–1158. Ye, P.; Shen, Y. R. *Phys. Rev. A* **1982**, *25* (4), 2183–2199.

(37) Williams, S.; Zare, R. N.; Rahn, L. A. *J. Chem. Phys.* **1994**, *101* (2), 1072–1092.

(38) Blum, K. *Density Matrix Theory and Applications*, 2nd ed.; Plenum Press: New York, 1981.

(39) Yee, T. K.; Gustafson, T. K. *Phys. Rev. A* **1978**, *18* (4), 1597–1617. Prior, Y. *IEEE J. Quantum Electron.* **1984**, *20* (1), 37–42.

(40) By invoking the slowing-varying amplitude approximation (see ref 3), the wave equation describing generation of the forward-going RFWM signal field can be written as:

$$\frac{\partial E_4(\omega)}{\partial \mathbf{r}} = \frac{i\omega}{2c\varepsilon_0}\boldsymbol{\varepsilon}_4^* \cdot \mathbf{P}^{(3)}(\omega)\mathrm{e}^{-i\mathbf{k}_4\cdot\mathbf{r}} = \frac{i\omega}{2c\varepsilon_0}\boldsymbol{\varepsilon}_4^* \cdot \tilde{\mathbf{P}}^{(3)}(\omega)\mathrm{e}^{-i\Delta\mathbf{k}\cdot\mathbf{r}}$$

where the factor $\mathrm{e}^{i\mathbf{k}_\sigma\cdot\mathbf{r}}$ appearing in our definition of the third-order polarization (eq 10), $\boldsymbol{\varepsilon}_4^* \cdot \mathbf{P}^{(3)}(\omega) = \boldsymbol{\varepsilon}_4^* \cdot \tilde{\mathbf{P}}^{(3)}(\omega)\mathrm{e}^{i\mathbf{k}_\sigma\cdot\mathbf{r}}$, leads to a net spatial dependence of $\mathrm{e}^{-i(\mathbf{k}_4-\mathbf{k}_\sigma)\cdot\mathbf{r}} = \mathrm{e}^{-i\Delta\mathbf{k}\cdot\mathbf{r}}$. For the small-signal limit obtained when incident beams propagate (with negligible modification) through an optically thin sample of length l, integration of the wave equation yields $E_4(\omega) \propto \boldsymbol{\varepsilon}_4^* \cdot \tilde{\mathbf{P}}^{(3)}(\omega)\mathrm{e}^{-ikl/2} l\,\mathrm{sinc}(\Delta kl/2)$, with the corresponding signal intensity given by $I_4(\omega) \propto |E_4(\omega)|^2 \propto |\boldsymbol{\varepsilon}_4^* \cdot \tilde{\mathbf{P}}^{(3)}(\omega)|^2 l^2 \mathrm{sinc}^2(\Delta kl/2)$. Momentum conservation or phase-matching criteria are reflected in the behavior of the $\mathrm{sinc}^2(\Delta kl/2)$ function, which peaks sharply (for finite l) at $\Delta k = |\Delta\mathbf{k}| = 0$ or $\mathbf{k}_4 = \mathbf{k}_\sigma$, where $\mathbf{k}_\sigma = \mathbf{k}_1 - \mathbf{k}_2 - \mathbf{k}_3$.

(41) Greene, C. H.; Zare, R. N. *Annu. Rev. Phys. Chem.* **1982**, *33*, 119–150. Greene, C. H.; Zare, R. N. *J. Chem. Phys.* **1983**, *78* (11), 6741–6753.

(42) Zare, R. N. *Angular Momentum: Understanding Spatial Aspects in Chemistry and Physics*; John Wiley and Sons, Inc.: New York, 1988.

(43) Redington, R. L. Coherent Proton Tunneling in Hydrogen Bonds of Isolated Molecules: Malonaldehyde and Tropolone. In *Hydrogen-Transfer Reactions (Vol. 1: Physical & Chemical Aspects; Part I: Hydrogen Transfer in Isolated Hydrogen Bonded Molecules, Complexes, and Clusters)*; Hynes, J. T., Klinman, J. P., Limbach, H.-H., Schowen, R. L., Eds.; Wiley-VCH Verlag GmbH & Co.: Weinheim, Germany, 2007; Chapter 1, pp 3−31.

(44) Burns, L. A.; Murdock, D.; Vaccaro, P. H. *J. Chem. Phys.* **2009**, *130* (14), 144304/1–16.

(45) Redington, R. L.; Redington, T. E.; Sams, R. L. *J. Phys. Chem. A* **2006**, *110* (31), 9633–9642.

(46) Nesbitt, D. J.; Field, R. W. *J. Phys. Chem.* **1996**, *100* (31), 12735–12756.

JP903970D